Interaction of Solid Earth, Atmosphere & Ionosphere

T. Tanimoto[1] and Juliette Artru-Lambin[2]

1. Department of Earth Science, University of California, Santa Barbara, California 93106

2. Centre National d'Etudes Spatiales, DCT/SI/IM-BPi 2111, 18 avenue Edouard Belin, 31400 Toulouse cedex 9, France

Version last modified on October 30, 2006.

Key Words

Interaction, Solid Earth, Atmosphere, Ionosphere, Noise, GPS

Abstract

The largest mechanical components of the Earth system are the solid body with two fluid envelopes: ocean and atmosphere. Each component in this system - the atmosphere, the oceans and the solid Earth - interacts with the others in complex ways on various time scales. The fluid envelopes generate mechanical noise in the solid body from which structural information can be retrieved because the Green's functions for the solid Earth can be constructed from such ocean- or atmosphere-generated noise. Likewise, various sources in the solid Earth generate waves that propagate in the atmosphere from which quantification of earthquakes, and volcanic sources are possible. Broadening the study of the solid Earth to include interactions with the fluid spheres will allow new data to inform and enrich traditional solid Earth science.

1 Introduction

The atmosphere has been traditionally ignored by seismologists in their analysis of seismograms. Seismologists typically regard the surface of the solid Earth as the upper boundary of the Earth and this boundary is treated as a traction-free boundary. The atmospheric pressure is not zero, however, and the correct boundary condition must reflect the existence of the atmosphere with its diminishing density with height. Strictly speaking, the actual physical upper boundary condition should be in the atmosphere as the radiation boundary conditions.

Despite this approximate treatment of the surface boundary, seismology has been successful mainly because of two factors. The first is that the impedance contrast at the atmosphere/solid earth boundary is quite large. Density contrast across this layer is larger than 2000 (1.2 vs. 2700 in kg/m^3) and P-wave velocity contrast is about 20 (300 vs. 6000 in m/s). If we take the case of P waves impinging on the solid surface from below, there is obviously some transmitted P wave energy but the majority of the energy is reflected back into the solid media due to this high impedance ratio. Resulting seismograms hardly indicate the effects of the leakage of transmitted energy.

The second important factor is the low mass of the atmosphere. The mass of the solid Earth is 6.0×10^{24} kg, while the mass of the atmosphere is only 5.1×10^{18} kg. Therefore, phenomena in the solid Earth are affected very little even if we include atmospheric effects in the analysis. It is thus justifiable to ignore the atmosphere and use the free-surface boundary conditions for many phenomena.

But does this mean that there are no benefits to include the atmospheric layer in the analysis? In a nutshell, the purpose of this chapter is to point out that there are many benefits to doing so. We can immediately think of two potential advantages; the first is the possibility of obtaining information on solid Earth processes from analyses of atmospheric waves. It has been pointed out that the eruption of Pinatubo volcano in 1991 generated air-coupled waves that provided information on the nature of the eruption process. Second, some earthquakes have been known to generate Rayleigh-wave coupled air waves which provide quantitative information on excitation source processes. These examples are analogous to the use of tsunami for the study of earthquake source process, because though tsunami themselves are mostly confined to the liquid layer (ocean), their level and of excitation often provides information about the slow rupturing process on an earthquake fault. Analyses of atmospheric waves have not been as useful as analyses of tsunami so far, but more careful studies of atmospheric waves may lead to useful applications to solid-earth processes.

Another benefit comes from the analysis of seismic noise. Most seismic noise in seismograms is generated by interactions between the solid earth and the atmosphere or the ocean. In the past 5-6 years, such noise was shown to be practically useful because we can recover Green's functions between any pair of stations using a cross-correlation technique. Its application to earth structure study is under way: seismic noise can provide surface wave dispersion curves between two stations and promise to provide results that were not available from earthquake data. The cross-correlation technique also provides information on the flow (direction) of propagating seismic energy, thereby providing potential information about the source location of noise, which was not possible to determine before.

This article consists of two main parts: In the first part, we will describe the nature of seismic noise and the Green's function cross-correlation technique. We will review the study of seismic noise and how noise illuminates our understanding of atmosphere-solid Earth interactions. Since the atmosphere and oceans are strongly coupled and often not separable, the oceans are involved in many of these processes.

In the second part, we will discuss events such as large atmospheric explosions or earthquakes, the effects of transient sources in the solid Earth, and the resulting effects in the atmosphere. These events radiate energy in various types of waves, such as seismic waves in the solid Earth, tsunamis in the oceans, and internal waves in the atmosphere. Dynamical coupling allows the transmission of a part of the wave energy across the sea or earth surface, hence the generation of atmospheric, ocean or tsunami waves from sources external to their respective domains. Sources of such coupled waves include (1) Atmospheric explosions, natural (meteors, volcanoes) or man-made, (2) Earthquakes, and (3) Sonic booms from supersonic jets (Concorde, Space Shuttle). Some notable effects observed after the great Sumatra-Andaman earthquake will also be discussed

The first and second parts take two different views on modelling the source-medium relationship. The first part follows the view that seismic waves generated by atmospheric effects are generated by surface atmospheric pressure variations. The Earth is basically separated in two distinct media in contact. In this view, generation of acoustic/gravity waves in the atmosphere by sources in the solid Earth are mainly by vertical surface displacement. On the other hand, the second follows the so-called full-coupling approach. There is no artificial boundary between the atmosphere and the solid Earth and the whole Earth is treated as a single medium. Normal modes are the normal modes of the whole system and propagating waves cross the atmosphere-solid Earth boundary just like other boundaries inside the Earth. In this view, sources are stress gluts or the Reynolds stresses. The approach in the first part is clearly an approximation but it seems to holds well.

2 Seismic Noise

Peterson (1993) summarized seismic noise characteristics from global distribution of 75 stations. One of the most frequently-quoted results from this study is the parametrized model called the New Low Noise Model (NLNM). Figure 1 shows a plot of this model in the form of acceleration power spectral density. This model has often been used as a reference in the discussion of seismic noise studies.

From the perspective of a seismologist, one of the main features in Figure 1 is the existence of a low noise frequency band from 2 to 20 mHz. Existence of this low-noise band explains why analyses of long-period body and surface waves have been successful in the past few decades as these waves exist in this low noise band (1 mHz - 10 Hz). Detection of small amplitude waves has been possible because of this low-noise characteristics which is not as easily done outside this frequency band.

From the perspective of a scientist interested in the atmosphere-solid Earth interactions, Figure 1 shows three prominent peaks; from the low frequency end, they are (1) the low frequency peak below 0.1 mHz, whose peak is outside the range of this plot but the decreasing trend with frequency up to about 2 mHz is clearly recognized, (2) a small peak or a bump at about 7-10 mHz (denoted as Hum in this figure) and (3) large amplitude peak(s) at 0.1-0.2 Hz (Microseims). In this section, we will discuss each of the three peaks from the low frequency end, particularly focussing on the question which components in the Earth system interacte to create these peaks.

The model NLNM was derived from vertical component seismograms. The noise in horizontal components is often an order of magnitude larger than the noise in vertical component because horizontal components are affected by tilts that are generated by temperature variations and atmospheric pressure variations. They are often dominant sources of noise in horizontal component seismographs but are confined to shallow depths and local regions. In this article, these noise in horizontal components will not be discussed.

2.1 Low frequency peak: Atmospheric Effects

Seismic noise below 2 mHz (milli-hertz) increase toward lower frequencies (Figure 1). This is a global feature that has been confirmed repeatedly from long-period seismographs and gravimeters.

2.1.1 Cause

The main cause of this noise is density changes in the atmosphere. For example, as weather patterns change, density changes occur in the atmosphere. These changes affect the gravitational field and generate small perturbations in gravitational acceleration at the surface of the Earth.

This mechanism was pointed out by Warburton and Goodkind (1977) by analyzing two co-located instruments, a barometer and a superconducting gravimeter. Barometric (surface pressure) data represent an integration of density anomalies along a vertical column above a station:

$$\Delta P = \int_0^\infty \Delta\rho g dz \tag{1}$$

where ΔP is the surface pressure perturbation, $\Delta\rho$ is density perturbation in this formula and the integration is from the surface of the Earth ($z = 0$) to infinity. Effects of atmospheric density perturbations above an observing station can be approximated by a formula similar to the Bouguer gravity formula:

$$\Delta g = 2\pi G \int_0^\infty \Delta\rho dz \tag{2}$$

where Δg is the perturbation to gravitational acceleration and G is the gravitational constant. Since g does not vary very much near the surface, barometric data and gravity data are related, to a good approximation, by

$$\Delta g = \frac{2\pi G}{g}\Delta P. \tag{3}$$

Warburton and Goodkind showed that co-located gravimeter data and barometric data correlate with coefficients close to a value predicted by $2\pi G/g$.

There is, however, an assumption in using the Bouguer gravity formula; in applying this formula, density perturbation in the atmosphere is assumed to be shaped like a disk-like pattern and density variations laterally away from the station location (in latitude and longitude) do not affect the gravitational acceleration very much. More careful evaluation of such effects, using a meteorological simulation model, showed that deviation from this formula is small (Boy et al., 1998; Hinderer and Crossley, 2000).

Changes in the atmospheric pressure also cause deformation of the elastic Earth as a surface load. Correction due to this effect is usually added to the above formula in the analyses (Warburton and Goodkind, 1977; Spratt, 1982; Van Dam and Wahr, 1987; Niebauer, 1988; Merriam, 1992; Crossley et al., 1995). This effect is not negligible and in fact was claimed to be larger than the above effect in earlier period of seismic noise study (Sorrells, 1971; Sorrells et al., 1971). But it is smaller than the righthand side of the above formula.

A clear demonstration of atmospheric pressure effects at the time of a cold front passage was documented by Müller and Zürn (1983) and some careful quantitative computational analysis was reported by Rabbel and Zschau (1985).

Figure 2 shows the evidence of correlation between gravity data and surface-pressure data after the removal of tidal signals from gravimeter data. The original gravity record (top) is dominatred by tidal signals but after their removal, the middle trace is obtained. This time series matches the barometric data at bottom closely, indicating peak-to-peak correlations between the middle trace and the bottom trace.

2.1.2 Turbulence

While it seems that the correlation between gravity (ground motions) and surface pressure data is good as shown in Figure 2, the correlation coefficient hovers around 0.5 and never becomes close to one. Uncorrelated part of the signal may be due to additional forces, such as wind stress (Reynolds stress) in atmospheric turbulence, which dominates the frequency range higher than above 1 mHz (Tanimoto, 1999). Frequency dependence of surface pressure in this frequency band shows the 1/f behavior as observed spectra in Figure 3 show (e.g., Tanimoto and Um, 1999). This 1/f behavior is consistent with the prediction by the theory of turbulence with the Kolgomorov-type scaling relation (Tennekes and Lumley, 1971; Landau and Lifshitz, 1987) and directly supports the importance of turbulence in this frequency band.

2.1.3 Reduction of Seismic Noise

Existence of the above mechanism suggests that, if a seismic/gravity instrument is co-located with a barometer, one can reduce the level of noise considerably by taking advantage of this correlation. For analyses of tidal and lower-frequency data, this has become a common practice since the study of Warburton and Goodkind (1977). For seismic data, especially for normal mode studies (about 1 mHz and above), Zürn and Widmer (1995), Beauduin et al. (1996) and Roult and Crawford (2000) showed significant noise reduction. These studies showed that noise level below 1 mHz can be made lower than the model NLNM by this correlation technique.

2.2 Hum

The second peak denoted by HUM in Figure 1 was identified as a broad peak by Peterson (1993). It was shown later that this peak is associated with multiple modal peaks, primarily on the lefthand side of its maximum. Figure 4 shows an example from data in this frequency range, obtained from global network data by averaging eleven stations located at various parts of the world. The bottom panel is an enlarged figure within the small box in the top panel and shows that modal peaks exist for the frequency range between 2 and 7 mHz. They are shown to match the eigenfrequencies of fundamental spheroidal modes almost exactly, as the eigenfrequencies for the Preliminary Reference Earth Model (PREM; Dziewonski and Anderson, 1981) are drawn in the bottom panel by vertical lines. These continuously excited modes are all fundamental spheroidal modes and do not seem to contain any overtone modes. They are now commonly referred to as the Earth's hum.

2.2.1 Discovery

Discovery of continuously excited modal peaks was made in 1997. A broad peak in Peterson's model has been noted since 1993, or perhaps even earlier, but the hum was discovered as an independent feature from it. The initial reports were by Suda et al. (1998), Kobayashi and Nishida (1998) and Tanimoto et al. (1998). These and subsequent studies showed that all sites where the noise level is as low as 10^{-18} (m^2/s^3) in acceleration spectral density (for the frequency-band 2-15 mHz) show signals of the Hum. Since the global minimum of horizontal noise is an order of magnitude higher than this value, all observations were from vertical component seismograms or gravimeters. The types of seismic intruments that led to these discoveries included broad-band seismometers STS-1 and gravimeters with spring sensor (Lacoste-Romberg gravimeters) or superconducting sensors. It was recently shown that seismic data from broadband seismometers STS-2 (with lower pendulum period than STS-1, about 100 seconds) at the Black Forest Observatory (BFO) in Germany show the Hum (Widmer-Schnidrig, 2003). This may not be surprising, however, since the noise level is as low as 10^{-18} (m^2/s^3) for STS-2 at this low-noise site. The most important point seems to be that the signal of the Hum are observed if the noise level is about 10^{-18} (m^2/s^3) or less, in unit for acceleration spectral density.

Nawa et al. (1998) reported the existence of the Hum in their superconducting gravimeter data at Showa station in Antarctica. Their report was made before the three papers cited above, but the reported results contain peaks from grave spheroidal modes (angular degree less than 10) that have not been confirmed independently. In addition, their later study (Nawa et al., 2000) showed that the noise level at this station seems to be much higher than 10^{-18} (m^2/s^3) for the frequency band 1-5 mHz.

2.2.2 Seasonal variations

These modal amplitudes display seasonal variations; claims of the predominant six-months periodicity were made by Tanimoto and Um (1999) from a frequency-domain analysis and by Ekström (2001) from an entirely independent time-domain analysis. A claim for an annual seasonality was made by Nishida et al. (2000), although they claimed that annual signal was dominant and was thus mildly different with the above two studies.

Detection of seasonal variations had major implications for the source of excitation of the hum because it basically removed causes in the solid earth, because phenomena in the solid Earth do not usually have clear seasonal signatures. Up until these discoveries on seasonality were made, slow earthquakes (e.g., Beroza and Jordan, 1990) were considered to be one of the major candidates for the cause of the hum.

2.2.3 Excitation mechanism

The cause of the Hum may be in the atmsophere or in the oceans. The atmospheric excitation was advocated by Kobayashi and Nishida (1998), Tanimoto and Um (1999) and Fukao et al. (2002). In these papers, pressure fluctuations in the turbulent atmosphere was postulated as the cause. Modal amplitudes of individual peaks were shown to be explained by the atmospheric excitation model. But there was an uncertain part in this scenario, particularly on the correlation length in atmospheric turbulence within the frequncy band (2-7 mHz range). This was critical because the excitation of modes by turbulent atmosphere is proportional to this parameter (Tanimoto, 1999; Goldreich and Keeley, 1977). The atmospheric excitation mechanism was advocated by assuming that this correlation length was about 1 km or larger for the frequency band 2-7 mHz. This correlation length has not been confirmed by observation although the existence of turbulent boundary layer of thickness 1 km seems to imply that it may be a viable candidate.

In addition to this uncertainty in source strength, the atmospheric excitation hypothesis does not provide a good reason for the existence of the broad noise peak between 3 and 15 mHz. In both Tanimoto and Um (1999) and Fukao et al. (2002), this broad spectral peak was assumed to be caused by an unknown background noise and only the modal peaks above this background noise were modelled by the atmospheric pressure variations at the surface.

The oceanic excitation hypothesis was advanced by Rhie and Romanowitz (2004) and Tanimoto (2005). Rhie and Romanowitz (2004) used seismic array data and located the sources of Rayleigh waves (noise) using two arrays in Japan and California. They found the excitation sources to be in the oceans, especially in the mid-latitude bands (30-60 degrees) in the northern and southern hemispheres. They also claimed that source locations switched rather abruptly between the northern and southern hemispheres. This feature seems to be compatible with general patterns of storm behaviors, although further independent confirmation is desirable.

Tanimoto (2005) showed that the overall spectral shape of the Hum, the modal peaks and the broad spectral peak depicted in Figure 1 (3-15 mHz) can be explained by a single mechanism if the oceanic infragravity waves were the cause. A rather ad-hoc feature in the atmospheric excitation hypothesis, which has to find separate causes for modal peaks and for the broad spectral peak, can then be avoided. Nishida et al. (2005) argues that it may still be possible to create this broad peak by atmospheric effects but a detailed mechanism is still missing in the atmospheric excitation hypothesis.

One of the uncertainties in the oceanic excitation hypothesis lies in our lack of knowledge on the oceanic infragravity waves. Limited number of observations (e.g., Watada et al., 2001) are now supplemented by new observations. Also, some new understanding as to the generation of infragravity waves from oceanic swells are emerging from observation (Dolenc et al., 2005). Although there have been some studies on the oceanic infragravity waves and many results (Webb et al., 1991; Okihiro et al., 1992; Dolenc et al., 2005) point to near-coastal generation of waves, a comprehensible, total picture of the generation mechanism seems to be missing. This is still an active research area.

Satellite ocean-wave data provide semi-hemispheric switching of activities, as shown in Figure 5. Ocean waves occasionally reach 10 m or more in high-activity regions which generates pressure perturbations higher than surface atmospheric pressure. This behavior seems to explain the six-months periodicity naturally as well as source locations of Rayleigh waves observed by Rhie and Romanowitz (2004). This satellite evidence does not necessarily prove the oceanic excitation mechanism for the HUM because strong atmospheric winds are associated with these ocean-wave behavior and the atmosphere also contains six-months periodicity. There is clearly an inherent difficulty in the argument of atmospehric vs. oceanic excitation because the atmosphere and the oceans are coupled in almost all scales.

2.2.4 Ubiquitous Rayleigh Waves

One of the most important notions developed in these studies is that the energy associated with the Hum, for the entire frequency range 3-15 mHz, consists of Rayleigh wave energy. From observation, Nishida et al. (2002) showed that signals between 2 and 20 mHz have similar phase velocities to Rayleigh wave phase velocities predicted by the Preliminary Reference Earth Model (Dziewonski and Anderson, 1981). Tanimoto (2005) showed that the whole spectra in this frequency band can be systhesized by normal mode summation of spheroidal modes, potentially excited by the ocenaic infragravity waves, thereby indicating that they are Rayleigh waves.

Along with the microseisms in the next section, a majority of seismic noise seems to be dominated by Rayleigh waves, at least those signals (noise) in vertical component seismograms.

2.3 Microseisms

It has been noted for a long time, since the early 20-th century, that the most obvious and perhaps annoying noise in seismograms are the microseisms with the peak frequency at about 0.1-0.4 Hz (Figure 1). Amplitudes of this noise was so overwhelming that, before the development of high-dynamic range digital seismic instruments, seismologists recorded seismic waves separately for high-frequency range (above about 0.5 Hz) and for low-frequency range (bvelow 0.1 Hz) in order to avoid this microseismic noise. World-Wide Standard Seismograph Network, which played the central role for the development of global seismology from 1960s to 1980s, had such separate (short-period and long-period) instruments.

Modern instruments with high dynamic range and digital recordings removed such a cumbersome recording procedure (Wielandt and Steim, 1986). They record seismic signals from about 1 mHz to 10 Hz using the same sensor. A benefit of such recording procedure is that microseisms are now recorded continuously and this has raised interests among some seismologists since we now have access to raw microseism data from modern high-dynamic range digital data.

2.3.1 Nature of Waves

Microseisms mostly consist of Rayleigh waves. This was shown by Lee (1935) and Haubrich et al. (1963) by particle motion analysis which indicated a charateristic retrograde elliptical particle motion. Later, array analysis (Lacoss et al., 1969; Capon 1972) showed that some higher-mode energy and Love wave energy were mixed in the signals. Earlier, Gutenberg (1958) also discussed two types of microseisms, apparently referring to predominant Rayleigh waves and occasional S waves. From modern three-component data, it is easy to confirm the dominance of Rayleigh waves in microseisms from phase velocity measurements from array observations (Lacoss et al., 1969; Capon, 1972) or from phase-shift observations between horizontal and vertical components which indicate mostly 90-degree phase shifts.

2.3.2 Excitation mechanisms

One of the important characteristics in microseisms is the fact that larger amplitudes occur for the double-frequency microseisms (0.1-0.4 Hz) than the primary-frequency microseisms that have the same predominant frequencies with ocean swells (0.05-0.07 Hz). It is still not clear why the double-frequency microseisms have such large amplitudes but the most widely accepted (basic) mechanism for the double-frequency microseisms is that of Longuett-Higgins (1950). Longuet-Higgins (1950) showed that interactions of two ocean waves in opposite direction can create the double-frequency microseisms through the nonlinear (advection) term in the Navier-Stokes equaiton. The crux of his theory is that, for surface displacement

ζ, pressure perturbation at sea bottom is given by

$$p(t) = \rho \frac{\partial^2}{\partial t^2}\{\frac{1}{2}\bar{\zeta^2}\}, \tag{4}$$

even when the depth extent of colliding waves, that make surface displacement ζ, do not reach the sea bottom. In fact, this pressure arises as a constant in the Bernoulli equation (Longuet-Higgins, 1950), implying that this pressure occurs at all depths. The bar denotes an averaging procedure over a wavelength. For example, if two ocean waves with the same frequency are propagating in opposite directions,

$$\zeta(x, t) = a_1 \cos(\omega t - kx) + a_2 \cos(\omega t + kx) \tag{5}$$

we get

$$p(t) = -\rho a_1 a_2 \omega^2 \cos(2\omega t) \tag{6}$$

from equation (4). This formula contains two important features; first, it shows the occurrence of double frequency pressure variations. These double-frequency pressure variations at sea bottom generate the double-frequency microseisms. Second, this formula shows that if there exists a unidirectional propagating wave, say $+x$ meaning $a_2 = 0$, this pressure term goes to zero because it is proportional to $a_1 a_2$. The double-frequency pressure variation requires existence of colliding waves. This mechanism was experimentally confirmed by Cooper and Longuet-Higgins (1951). Phillips (1977) showed a derivation of the same formula from the Navier Stokes equation by carefully analyzing the vertical momentum balance.

Hasselmann (1963) cast the problem in a more general context, expressing the ocean wavefield as a wavenumber integral, and then showing that the predominant term is equivalent to the Longuet-Higgins formula. Normal mode excitation analysis of seismic wavefields by nonlinear interactions of ocean waves also showed recently that the Longuet-Higgins pressure formula naturally arises from the analysis (Tanimoto, 2006).

2.3.3 Source location

While it is clear that nonlinear interaction of ocean waves is necessary to generate microseisms, there is some confusion as to exact locations of excitation sources. This is partly due to the fact that the Longuett-Higgins' mechanism is effective at any depth; regardless of ocean depths, the pressure in the above formula is transmitted to the ocean bottom. What we know for sure is the fact that a source must be a place where ocean-wave collisions occur. This leads us to two potential locations; one is a coast where we can expect some reflected ocean waves from a coast can collide with incoming ocean waves. The other is an eye of low pressure systems.

Close relationship between microseisms and ocean swells near the shore was shown by Haubrich et al. (1963) and more recently by Bromirski et al. (1999). The latter involved a correlation study between microseisms from seismograms and ocean waves from buoy data and demonstrated a high correlation and thus a causal relationship.

On the other hand, it seems also true that storms provide a condition that ocean waves collide from opposite directions near their eyes. Tracking of a storm was done by Santo (1960), Sutton and Barstow (1996) and Bromirski et al. (2001) in order to understand the source process of the double-frequency microseisms. The work by Bromirski et al. (2001) provided the most quantitative analysis and reported that the dominant source area for the double-frequency microseisms was not in the open ocean, where the highest waves occurred, but were near the coast. It seems therefore that standing ocean waves that occur near the coasts, even at the time of large low pressure system, are the source of double-frequency microseisms. This does not mean that the eye of the low pressure system does not send out seismic waves; it simply seems to be dwarfed by near-coastal processes.

Friedrich et al. (1998) peformed a careful array analysis of seismic data and reported that the primary microseisms contained more Love waves than the double-frequency microseisms, suggesting that the exciting mechanisms may be quite different between them.

It has also been noted that source area of primary microseims is often spread out along the coasts whereas source areas of the double-frequency microseisms appear to be specific locations. This was observed in Europe (Friedrich et al., 1998), on the Atlantic coast (Bromirski et al., 2001) and the Pacific coast of the United States (Bromirski et al., 1999; Schulte-Pelkum et al., 2004). Also Schulte et al. (2004) showed a temporary effect of microseismic signals in California caused by ocean waves on the Atlantic coasts, although occurrence of such phenomena does not seem to be common.

In summary, there is still confusion as to the exact locations of excitation but the importance of near coastal region has become clear, at least for double-frequency microseisms.

2.3.4 Microbaroms

Microbaroms are atmospheric low-frequency waves, having frequencies close to those of double-frequency microseisms. Similarity of power spectra to those of microseisms suggest that they are of the same origin (e.g., Donn and Naini, 1973; Nishida et al., 2005). Posmentier (1967) presented a theory analogous to the mechanism proposed by Longuet-Higgins (1950). Arendt and Fritts (2000) published a more complete theory, carefully analyzing various types of waves that arise from interactions of ocean waves. The basic mechanism in both studies is the same with the Longuett-Higgins mechanism for microseism generation and assume interactions of two surface waves propagating in opposite directions. Standing ocean waves near the coasts appear to be generating both microseisms and microbaroms.

2.3.5 Implication to Past Climate

Changes in the climate are likely to be related to ocean wave behaviors (Bromirski et al., 1999; Bromirski and Duennebier, 2002), which may threaten coastal areas if they become too energetic. However, recovery of past ocean wave heights from meteorological data is generally difficult. Greyvemer et al. (2000) proposed to use activities of microseims in historical seismograms as a proxy for obtaining information for historical ocean wave behavior. They reported that the number of high microseismic days increased from 7 days to 14 days in the last 50 years and suggested that this may be related to global warming indirectly. While this result should be regarded as preliminary, it is reasonable to expect some correlation and microseism records may turn out to be a useful source of information for ocean-wave behavior and thus for climate changes.

2.4 From Noise to Structure

One of the motivations to study seismic noise is its potential use for earth structure study. Many techniques have been developed, each focusing on different aspects of data; examples include, in historical order, spatial variation of correlation amplitudes, array analysis for Rayleigh-wave phase velocity measurements, use of horizontal-vertical amplitude ratios for Rayleigh wave signals and the two-station correlation technqiue to recover the Green's functions between a pair of stations. Below we first discuss the most recent development, the correlation technique to recover Green's functions in diffuse seismic wavefields, and then discuss other techniques under classification as the traditional methods.

2.4.1 The Correlation Technique in Diffuse Wavefield

The first application of the correlation technique to recover structural information was demonstrated in helioseismology (Duvall et al., 1993). The essence of the technique was to recover travel time vs. distance curve for multiply reflected waves through cross-correlation of data at various distances. In the case of the Sun, seismic sources are stochastic in time and space, and thus there are no specific noise sources; it can be anywhere and any time. Therefore, such a technique was most needed and worked effectively to get the results.

Applications to other fields, such as geophysical exploration (Rickett and Claerbout, 1999) and ultrasonics (Weaver and Lobkis, 2000), followed before seismology adopted it recently (Campillo and Paul, 2003). Theoretical basis to recover the Green's functions from noise was discussed in Weaver and Lobkis (2001), Lobkis and Weaver (2001), van Tiggelen (2003), Malcolm et al. (2004), Snieder (2004), and Roux et al. (2005a).

Applications to seismic data started with Campillo and Paul (2003). Recovered signals were dominated near the microseismic frequency bands (about period 5-10 seconds) in earlier demonstrations. The technique was soon applied to local to regional scale problems such as Southern California (Shapiro et al., 2005; Sabra et al., 2005). It is now applied to much wider frequency bands (up to 100 seconds in period) and is also applied to continental scale structure.

Typical seismic applications first recover the Green's functions by cross correlation of seismograms at two stations. Since data are mainly from vertical components and are dominated by Rayleigh waves, traditional dispersion measurements for group velocity are often used to retrieve earth structure. Dominance of fundamental-mode surface waves in noise is perhaps unavoidable because the excitation sources are in the atmosphere and the oceans, although there are now some studies which report successful recovery of body wave signals (e.g., Roux et al., 2005b). This is currently a rapidly expanding field and the landscape of the research field is expected to change quickly in a few years.

2.4.2 Traditional Techniques

Aki (1957, 1965) proposed a method, often referred as the Spatial Autocorrelation method (SPAC), to determine local seismic structure. This technique also uses the cross-correlation among stations but focuses on amplitude variations of the correlated signals in space; in a flat layered media, the correlation function becomes proportional to bessel functions (Aki, 1965) from which one can obtain phase velocity. Therefore, it is quite different from the above correlation technique that focusses on phase information.

Töksoz (1964) and Lacoss et al. (1969) showed that an array-based phase velocity measurement is a powerful approach. This is basically a beamforming technique, using array data, and is becoming increasingly popular because of availability of dense seismograph networks.

Both SPAC and the beamforming approach are still used at present and an enormous body of literature exists in this area, especially in geotechnical engineering. In geotchnical engineering, the frequency range extends up to 10-20 Hz, exceeding the microseismic frequency band (0.1-0.4 Hz). These studies not only use microseismic signals but higher frequency signals generated by other sources and can only be called a cultural noise. A good recent summary of this field was given by Okada (2003).

These traditional techniques have been around 40-50 years but their practical use may expand as quality and density of seismic instruments have improved recently. We expect to see more use of these methods because there are urgent needs, especially in urban area, to understand near-surface structure as shallow seismic structure plays a critical role for ground motion amplification at the time of major earthquakes.

3 Localized sources of interactions

In this section we will focus on the interaction between the solid Earth and the atmosphere after localized and transient events such as earthquakes and volcanic eruptions.

3.1 Historical Context

An early example of observations can be traced back to more than a century ago, the eruption of the Krakatoa volcano (Indonesia) on August 26, 1883. After the eruption, coupled air-sea waves were observed in barographs and tide gauges worldwide (Harkrider 1967). The meteor or comet explosion in Tunguska (Central Siberia) on June 30, 1908 also induced both atmospheric and seismic waves. The latter was similar in amplitude to a M=5 earthquake (Whipple, 1930), although the true source of those waves was an explosion in the air, at an estimated altitude of 8 km (Ben-Menahem, 1975).

The interest for the study of such interactions rose significantly later, during Cold War periods, because atmospheric gravity waves were emitted by nuclear explosions and detection and characterization of such waves became an active research field (Hines, 1972). This led to three major advances during the 1960s. First, a better and efficient theoretical description of internal waves in the atmosphere (Hines, 1960), from the ground up to ionopsheric heights, was developed. Second, ionospheric sounding networks capable of monitoring the ionospheric response to those waves (Davies, 1962) were deployed. And third, the occurrence of several major earthquakes (Chile, May 22, 1960, M9.5; Alaska, March 28, 1964, M9.2) revealed the generation of internal acoustic waves in the atmosphere by global Rayleigh wave propagation (Donn, 1964).

More recently, significant advances were made toward a quantitative interpretation and prediction of such coupled phenomena. In particular, new types of atmospheric observations have been made possible by the development of GPS (*Global Positioning System*) ionosphere monitoring (Mannucci et al., 1998; Calais and Minster, 1998) and by the deployment of the International Monitoring System (global seismological, hydroacoustic, radionuclide, and infrasound network aimed at ensuring compliance with the Comprehensive Nuclear-Test-Ban Treaty). Increased accessibility of numerical computations has also made it possible to refine theoretical modeling of coupled systems (LePichon et al., 2003; Artru et al., 2004).

3.2 Theoretical Preliminaries

3.2.1 Wave propagation in the atmosphere

After localized events, energy is transmitted in the form of atmospheric internal waves from the surface to the ionosphere. Those waves arise from the interactions of compressional and gravitational forces and are divided into two classes, long-period gravity waves and short-period acoustic waves. The basic physics of acoustic-gravity waves was formulated by Hines (1960), and his formalism is now widely used. Let us review the main features of this theory.

We consider an isothermal atmosphere, initially in hydrostatic equilibrium, and include forces from inertia, gravity, and pressure gradients. We assume that disturbances can be regarded as adiabatic process because wave propagation is a sufficciently fast process. We do not include the effects from the rotation of the Earth, and therefore large-scale tidal and planetary waves are not considered here. We focus on much shorter-wavelength waves.

Let us use the notations that ρ is the density, p is the pressure, $\mathbf{v}$ is the neutral gas velocity, $\mathbf{g}$ is the gravitational acceleration and C_s is the constant sound speed. We then have the following three basic equations:

Conservation of mass:

$$\frac{\partial \rho}{\partial t} + \mathbf{v} \cdot \nabla \rho = -\rho \nabla \cdot \mathbf{v} \tag{7a}$$

Conservation of momentum:

$$\frac{\partial \mathbf{v}}{\partial t} + \mathbf{v} \cdot \nabla \mathbf{v} = \mathbf{g} - \frac{1}{\rho} \nabla p \tag{7b}$$

Adiabaticity:

$$\frac{\partial p}{\partial t} + \mathbf{v} \cdot \nabla p = {C_s}^2 \left(\frac{\partial \rho}{\partial t} + \mathbf{v} \cdot \nabla p \right) \tag{7c}$$

In the equilibrium state, $\mathbf{v}_0 = 0$ and both ρ_0 and p_0 are proportional to $\exp(-z/H)$, where $H = {C_s}^2/\gamma|\mathbf{g}|$ is the density scale height and γ is the specific heat ratio. Assuming ρ_1, p_1, and $\mathbf{v}$ are small perturbations with no dependency on the y-axis, we may solve the linearized equations as harmonic solutions by assuming that ρ_1, p_1 and $\mathbf{v}$ are proportional to $\exp\left[i\left(\omega t - k_x x - k_z z\right)\right]$. The full dispersion relation takes the form:

$$\omega^4 - \omega^2 C_s^2\left(k_x^2 + k_z^2\right) + (\gamma - 1)\, g^2 k_x^2 + i\gamma g \omega^2 k_z = 0 \tag{8}$$

This equation means that, in the presence of gravity, no solution exists in which both k_x and k_z are purely real and different from zero. Let us assume that k_x is real and seek a solution that propagates in the x direction as a harmonic wave. There are now two possibilities, either k_z is purely imaginary or

$$k_z = k'_z + i\frac{\gamma g}{2c^2} = k'_z + i\frac{1}{2H}. \tag{9}$$

The first case (k_z pure imaginary) is appropriate for horizontally propagating surface waves but it permits no variation of phase with height. The second case is appropriate for travelling disturbances in the atmosphere under the influence of gravity. Thus the second case is pursued here. The dispersion relation can be rewritten as:

$$\omega^2 {C_s}^2 {k'_z}^2 = \omega^4 - \omega^2\left({C_s}^2 {k_x}^2 + \frac{\gamma^2 g^2}{4{C_s}^2}\right) + (\gamma - 1)\, g^2 k_x^2 \tag{10}$$

For a given horizontal wavenumber, a real solution for k'_z exists only when the righthand side of equation (7), which is a second order polynomial in ω is positive. The two roots ω_1 and ω_2 define the following three different cases:

- If $\omega_1 < \omega < \omega_2$, k'_z is purely imaginary. In this case we can only have waves trapped at the surface propagating only horizontally (Lamb waves).

- If $\omega < \omega_1 < (\gamma - 1)^{1/2} g/C_s$, k'_z is purely real; this correspond to the internal gravity waves domain, governed primarily by buoyancy. $\omega_g = (\gamma - 1)^{1/2} g/C_s$ is the Brunt-Väisälä frequency.

- If $\omega > \omega_2 > \gamma g/2C_s$, k'_z is purely real; this correspond to the internal acoustic waves domain, governed primarily by compression. The high frequency limit of those waves is usual sound wave (with exponential increase in amplitude). $\omega_a = \gamma g/2C_s$ is called the acoustic cut-off frequency. In the short-wavelength limit, however, the root ω_2 varies as $C_s k_x$.

Typically $\omega_a/2\pi = 3.3$ mHz and $\omega_g/2\pi = 2.9$ mHz in the lower atmosphere. This classification in acoustic, gravity and Lamb wave is widely used in aeronomy. It can be extended to non-isothermal models when the scale height is large in comparison to the vertical wavelength. An adaptation of normal-mode theory to such a non-isothermal model, for the coupled solid Earth-ocean-atmosphere system, has been developed which allows simulation of wave propagation for the whole system (Lognonne et al., 1998). The main difference with traditional seismic normal-mode simulation is in the treatment of the upper boundary condition to reflect the absence of free surface.

Attenuation of waves arise from viscous and thermal dissipations with comparable magnitudes. But except for short-period acoustic waves, attenuation can be neglected up to 100 km of altitude. This is because dominant atmospheric waves that are coupled to Rayleigh waves have frequency content of about 10-20 mHz.

Stronger limitations of this model arise at high altitude because of two reasons; first, amplification with altitude implies that linearized equations will cease to be valid. And second, upward-propagating internal waves eventually reach the ionosphere, where the dynamics is strongly constrained by the influence of magnetic field on charged particles. The ionospheric response to gravity waves is still an object of an extensive literature (Yeh and Liu, 1972).

3.2.2 Frequency-Wavelength domains of interest

Seismic, tsunami and atmospheric waves result from the action of gravity and elastic forces. Significant effects from both types of forces exist for the relevant frequency range (a few tens of millihertz). Figure 6 represents a normal-mode representation of the whole Earth + ocean + atmosphere system (Lognonne et al., 1998; Artru et al., 2001). The range of existence of seismic, tsunami, acoustic and gravity waves can be clearly identified, and the different areas where they coexist (seismic and acoustic, tsunami and gravity) mark the potential for coupled waves. Outside those area, the dynamic coupling is limited to interface waves (*e. g.*, Lamb wave in the atmosphere).

Study of atmospheric signals caused by sources in the solid Earth is mostly based on observations at the surface (seismograms, barograms, tides gauges, infrasound arrays), or at high altitudes through the ionospheric response to upward-propagating internal waves. The latter measurement can only concern the acoustic or gravity frequency ranges. In particular, seismic and tsunami waves are much more likely to produce strong atmospheric signals at high altitude than many other natural or artificial sources. This is because, despite the very small size of displacements at the surface, they present a unique combination of frequency and horizontal wavelength range necessary for an efficient coupling with internal waves in the atmosphere. On the other hand, major energy from ocean swell, located in the same frequency range, may induce some infrasonic signal trapped at the base of the atmosphere (Garces et al., 1993), but will not in general induce internal (*i.e.* upward propagating) acoustic waves in the atmosphere, because the wavelength is much shorter than for Rayleigh waves (Arendt and Fritts, 2000).

3.3 Observation techniques

3.3.1 Surface observation: seismometer, microbarograph, hydrophones

Both seismic and pressure sensors have been used to characterize the coupling at the earth surface. In particular, recent worldwide deployment of infrasound arrays for the International Monitoring System has enabled us to detect atmospheric pressure fluctuations related to solid Earth activity (Fig. 7). The frequency band for such instruments is typically between 0.1 and 10 Hz (Muschlecner and Whitaker, 2005). The noise level depends on the wind conditions, from 0.1 to 10 Pa, but it can be reduced by filtering. Those arrays can also be used to determine the azimuth and velocity of the observed signals, which provide information on their origin. Essentially two types of infrasound signals are observed after earthquakes (LePichon et al. 2002):

- Seismic coupled air waves, essentially a local conversion of seismic wave vertical motion into sound pressure (Donn 1964).
- Infrasound waves remotely generated. Those can be generated at the epicenter (Bolt 1964) or backscattered by mountain ranges (Young and Green, 1982).

In the latter case, infrasounds travel obliquely upward in the atmosphere but are reflected or refracted at various altitudes because of sound velocity variations in the atmosphere (Drob et al. 2003). Such a signal arrives later than the coupled air wave, and has different azimuth and velocity. Muschlecner and Whitaker (2005) showed that amplitude of the observed pressure perturbations depend not only on the epicentral distance and magnitude of the earthquake but also on the stratospheric wind speed, which has a major impact on the propagation of infrasounds.

3.3.2 High altitude observation: ionosondes, Doppler sounding, transmission (GPS), in-situ

Detection of acoustic and gravity waves at intermediate altitudes in the neutral atmosphere is not possible due to the absence of in-situ measurement and because atmospheric remote sensing generally lacks the resolution that would be needed. However, at higher altitudes, in addition to the exponential amplification of the wave amplitude, the interaction with the local plasma leads to perturbations of the ionosphere that are detectable by using radio sounding techniques.

The ionosphere is the intermediate region between the neutral atmosphere and the magnetosphere, ranging approximately between 60 and 1500 km in altitude. It is a stratified medium, partially ionized by solar radiation (due to ultraviolet light and X-rays). The maximum in electron density is reached between 200 and 400 km of altitude, and takes values between $10^5 - 10^7$ e^-m^{-3} (Fig. 8).

Because it is a plasma, the ionosphere has a strong influence on electromagnetic waves propagation. The plasma frequency is the low frequency cut-off for radio wave propagation, and depends on the local electron density N_e as:

$$\omega_p = \left(\frac{N_e e^2}{m_e \epsilon_0}\right)^{\frac{1}{2}}, \tag{11}$$

where e and m_e are the electron charge and mass, and ϵ_0 is the permittivity of vacuum. Typical ionospheric plasma frequencies range from 1 to 20 MHz and their maximum occurs at the maximum of ionization. Ionospheric sounding techniques are based on measurement of either the reflection of radio waves below the maximum plasma frequency, or the refraction delay of higher frequency signals transmitted across the ionosphere from satellites.

Reflection For frequencies lower than 10 MHz, waves are reflected by the ionospheric layer whose plasma frequency (Eq. 11) exceeds the frequency of signal. One type of radio sounding of the ionosphere is vertical sounding (ionosonde), measuring the travel time of a reflected signal as a function of frequency. This provides information on the electron density profile. Doppler sounding is based on the measurement of the Doppler shift of monochromatic signal, sent vertically upward and reflected back to the ground. The frequency shift between the emitted and the reflected wave is directly proportional to the vertical velocity of the reflecting layer. Using such ionospheric sounding network, Blanc (1985) gave a review of natural and artificial sources of signals recorded in those "ionospheric seismometers". Both types of sounding can be either ground-based, probing the lower ionosphere up to the electron density maximum, or satellite-based ("top-side sounding").

Transmission For higher frequencies (typically L-band, 1-2 GHz and higher), electromagnetic waves can propagate across the ionopshere. Ionospheric refraction induces a delay in the traveltime, which depends on the frequency of the signal and on the local plasma frequency (equation 11), hence on the local electron density along the ray:

$$\delta\rho_{iono} = \pm\frac{e^2}{4\pi^2 m_e \epsilon_0}\int_{ray}\frac{N_e}{f^2}dl \tag{12}$$

Using traveltime measurements at two different frequencies gives access to the Total Electron Content (TEC), which is the integral of electron density along a path between a radio transmitter and a receiver. This measurement on TEC has become widely accessible from the development in satellite altimetry and positioning, since it is a key correction required to be applied to those systems. In particular, Global Positionning System (GPS) relies on the accurate measurement of satellites - GPS receiver distances and uses a combination of traveltime measurements at two frequencies (L1 and L2, respectively $f_1 = 1.575$ and $f_2 = 1.227$ GHz). Once other sources of error are taken into account (Lanyi and Roth, 1988;

Sardon et al., 1994), TEC along the ray can be obtained as a linear combination of the two estimated distances ρ_1 and ρ_2:

$$TEC = \int_{ray} N_e \, dl = \frac{1}{40.3} \frac{f_2^2 - f_1^1}{f_2^2 \, f_1^2} \left(\rho_1 - \rho_2\right). \tag{13}$$

3.4 Sources in the solid Earth

Ionospheric perturbations that follow earthquakes have been observed both near the seismic source and at teleseismic distances (Fig. 9). The first published observations were related to the great Alaska earthquake in 1964. Using ionospheric sounding networks, Bolt (1964) and Davies (1965) observed atmospheric perturbations propagating from the epicenter region and the ionospheric signatures of the Rayleigh wave propagation at the sounder location.

3.4.1 Away from the source: surface waves and tsunamis

Seismic waves Seismic surface waves have typical group velocity in the range $3-4$ km.s^{-1}, whereas the sound velocity in the atmosphere is much smaller (340 m.s^{-1}). Therefore, the acoustic wave is sent almost vertically upward and reaches the ionosphere with a delay of 8-15 minutes after the passage of Rayleigh waves on the ground. Amplification due to density decrease with altitude can reach 10^4 to 10^5, and attenuation is only observed for short-period signal above 100 km of altitude. Large-scale vertical oscillations of the ionospheric layers can be easily monitored using the Doppler sounding networks described in section 3.3.2 (Yuen et al., 1969; Blanc, 1985). Figure 10 presents a recent example of such measurements. Although monitoring networks are still sparse, such ionospheric oscillations are currently observed systematically for most M$\geq$ 6.5 earthquakes worldwide.

Using a normal-mode approach, Artru et al. (2004) have modelled oscillations of ionospheric layers induced by surface Rayleigh waves generated by a major earthquake. Their analysis retrieved source parameters from atmospheric events and showed that atmospheric perturbations generated by surface Rayleigh waves may be amplified by a factor of 10,000 to 100,000 upon attaining heights between 150 and 250 km.

Tsunami waves Tsunami waves are expected to induce a similar type of coupling with the atmosphere; despite their small amplitude compared with ocean swells, they can generate atmospheric gravity waves because of their long wavelengths. A possibility of detecting tsunami by monitoring the ionospheric signature of the induced gravity waves was proposed by Peltier and Hines (1976). They discussed theoretical issues on the coupling and concluded that it is feasible.

Geometry of tsunami-gravity wave coupling is very different from the coupling between seismic and acoustic waves. Tsunami wave is non-dispersive, and its velocity depends only on gravity g and water depth d, as the velocity is given by $\sqrt{gd}$. From the gravity wave dispersion equation, one can estimate group velocity of the induced gravity wave. Horizontally, it appears to be very close to typical tsunami wave speed, while vertical component is much slower than sound speed (about 50 m/s). Depending on the period, it would therefore take from one to a few hours for the gravity wave to reach the ionosphere (in contrast to about 10 minutes for seismic-acoustic waves). The ionospheric perturbation should be behind the tsunami front, with a delay increasing with altitude.

Early papers that proposed using ionospheric measurements to detect tsunami-generating earthquakes (Najita et al., 1973; Najita and Yuen, 1979), focused on perturbations induced by Rayleigh waves preceeding a potentially destructive tsunami. Artru et al. (2005) used ionospheric sounding from a very dense GPS network in Japan (GEONET) to detect the perturbations associated with the arrival of tsunami wave, generated by the June 23, 2001 Peru earthquake. The observed arrival time, wavelengths and orientation were shown to fit well with theoretical predictions estimated by a simple simulation (Fig. 11).

3.4.2 Direct atmospheric waves

Atmospheric perturbations, observed either at the ground level or in the ionosphere, are often generated away from the measurement location. Propagation of the signal is therefore essentially in the atmosphere. In most cases, the origin of the atmospheric disturbance is the ground motion near an earthquake source (or an underground nuclear explosion). Calais and Minster (1995) detected perturbations in the ionospheric total electron content above

Southern California after the Northridge earthquake (M=6.7, January 17, 1994) using GPS measurements. Davies and Archambeau (1998) developed a direct modeling of these waves for a simple representation of shallow seismic sources, including high-frequency components of the wave-packet and nonlinear effects. Their results confirmed the seismic origin of the signal, observed after the Northridge earthquake.

The displacement field generated at the Earth's surface produces a piston-like impulse on the atmosphere. Afraimvich et al. (2001) proposed a model for the atmospheric perturbation in the form of "shock-acoustic waves". Drob et al. (2003), Il-Young et al. (2002), and Virieux et al. (2004) focused on solving the acoustic wave propagation in order to model data from CTBT verification network.

Other sources of infrasounds In addition to the coupled surface waves and the direct acoustic-shock waves, some atmospheric perturbations related to earthquakes can be observed as scattered waves away from the source. For example, a mountain range can become a source of diffracted infrasound waves at the time of passage of Rayleigh waves (LePichon et al., 2002; LePichon et al., 2003; Mulschlecner and Whitaker, 2005).

Other "solid Earth" sources of atmospheric infrasounds include avalanches and rockfall (Bedard, 2000), volcanic activity (Garces et al., 1997), and chemical explosions and mining blasts (Hagerty et al., 2002).

3.5 The case of the Great Sumatra-Andaman earthquake

The great ($M_w = 9.1$) Sumatra-Andaman earthquake and tsunami of December 26^{th}, 2004 (Lay et al., 2005) provided a unique opportunity to study solid Earth-ocean-atmosphere coupling. Indeed, by itself this particularly large thrust event would generate not only seismic wave and their associated atmospheric Rayleigh wave, but also direct atmospheric perturbation. In addition it triggered an exceptionally large tsunami that propagated across the Indian Ocean. Satellite altimetry observation could detect the open-ocean wave, with peak-to-peak amplitude of 40 to 50 cm (Song et al., 2005). Tide gauge stations also provided tsunami data, allowing Tanioka et al. (2006) to estimate the rupture process somewhat independently from purely seismic data. The propagation of the tsunami wave across the

Indian Ocean lasted for several hours, which was enough, according to the tsunami-gravity wave coupling theory described earlier, to generate ionospheric signal. Let us review some recent observations published on the subject, although some other works might still be under progress and unpublished at this time.

Le Pichon et al. (2005) and Garces et al. (2005) analyzed infrasound array data: they observed distinct packets of signal arriving successively: firstly the pressure perturbation generated at the sensor location by the seismic waves, with horizontal trace velocity greater than 3 km/s, and secondly an infrasonic wave train with a mean trace velocity of 0.35 m/s and a dominant period of 10s, associated with infrasound radiated from the epicenter region. A third sequence consisted in large coherent infrasonic wave, similar in velocity as the previous train, with a dominant period of 30s, for with back azimuth reconstruction indicate a source area extending from the northern tip of Sumatra to the northern margin of the Bay of Bengal: this suggests that those infrasonic waves were generated by the tsunami wave, either through the interaction of the tsunami with the shoreline, or as the tsunami reaches shallow water and presents shorter wavelength (a few tens of kilometers, comparable to 30s infrasound waves).

At higher altitudes, ionospheric perturbations related to the Sumatra earthquake and tsunami have been reported as well. Liu et al. (2006a) used Doppler sounding network in Taiwan, monitoring the vertical motion of a specific ionospheric layer, and detected two distinct disturbances interpreted as the Rayleigh acoustic wave, then to the direct acoustic-gravity wave emitted by the crustal motion around the earthquake. Other works published were based on continuous GPS data (*i. e.* the detection of perturbation in the integrated electron content of the ionosphere), although the distribution of permanent receivers in the Indian Ocean region was quite scarce at the time. Heki et al. (2006) studied the signals related to the direct acoustic-gravity wave from the source region and used such observation to retrieve information on the rupture process, in particular the rupture propagation speed. Using sensibly the same GPS stations in Sumatra and Thailand, Otsuka et al. (2006) focused on the variations in the TEC perturbation observed between different stations, interpreted as the consequence of the directivity in the ionospheric response with respect to the neutral atmosphere perturbation. DasGupta et al. (2006) reported smooth variations in TEC detected by GPS stations located on the East coast of India without giving yet any specific interpretation for their origin. Iyemori et al. (2005) reported a rather different kind of observation, using ground-based fluxgate magnetometer. They observe localized, long period geomagnetic pulsation in Thailand shortly after the origin time of the earthquake and speculated that it was due to the resonant interaction of magnetic field lines with the upward propagating magnetosonic wave emitted from the earthquake area.

Searching for ionospheric disturbances related to the tsunami wave propagation, two works reported some successful observation: Liu et al. (2006b) used GPS data from 5 permanent receivers in the Southern Indian Ocean and detected TIDs with period in the range 10-20 minutes, with horizontal propagation speed consistent with the theory of tsunami-gravity wave coupling. Occhipinti et al. (2006) took advantage of the simultaneous sea surface height and TEC measurements provided by altimetry satellites Jason-1 and TOPEX/Poseidon, hence giving data in the open ocean, away from possible coastal perturbation. In addition, they were able to perform a direct 3D modeling of the tsunami-generated gravity wave including its interaction with the ionospheric plasma. The simulated and observed perturbations agreed remarkably well considering the large uncertainties inherent to the combination of data, models and theory from very different fields of Earth sciences.

3.6 Sources in the atmosphere

Atmospheric events that generate infrasounds or gravity waves radiate in some cases enough energy to induce seismic signals through a dynamic coupling and the inverse energy flow from the atmosphere to the solid Earth can occur. Two main categories are discussed below; volcanic eruptions and sonic booms. The latter include data from the shuttle, supersonic jets or meteors that enter into the atmosphere.

3.6.1 eruptions

Atmospheric waves produced by the Krakatoa eruption in 1883 were observed worldwide by barometric measurements. The propagation of such atmospheric disturbances is similar to those produced by nuclear explosions, and investigations were made in the 1960's to characterize these waves and their impact on the ionosphere (Row, 1967; Harkrider, 1967). Following the eruption of Mount St. Helens in 1980, Roberts et al. (1982) detected a long-lived, large-scale traveling ionospheric disturbance in TEC measurements. Bolt and Tanimoto (1980) reported air waves in barograph records that circled more than once around the globe. The eruption of Mount Pinatubo (Philippines) on June 15, 1991 provided a remarkable example of the interaction between the solid and gaseous envelopes of the Earth system. The energy released in several explosions is estimated to be more than 100MT (TNT), generating significant atmospheric pressure waves (see Fig. 6). Signals related to these waves were observed worldwide in barographs, ionograms, Doppler soundings, TEC measurements, and seismic data, resulting in multitude of analyses for different data. Igarashi et al. (1994) used the Japanese ionospheric observation network to determine the characteristics of the gravity wave and the associated traveling ionospheric disturbances. Kanamori et al. (1994) investigated the source mechanism of atmospheric oscillations from both barographic and seismographic records. Johnson (2003) gave a review of infrasound observations emitted from volcanic eruptions and pointed out that it is to distinguish regular seismic signals related to sub-surface seismicity from the seismicity associated with gas release.

3.6.2 sonic boom

Seismic and underwater perturbations induced by aircraft sonic booms have been studied since the mid-1960s (Cook et al., 1972). Frequency range is much higher than those for previously discussed phenomena. It should be noted that these sonic booms are one of the rare examples of controlled sources. The main effects of sonic booms arise in the waveforms of the strain with the shape of the N-wave overpressure, and also in air-coupled Rayleigh wavetrains following each N-wave transient. Seismic waves generated by the coupling can then propagate, faster than the original shock wave (Ishihara, 2003). More recently, the Concorde (LePichon et al., 2003) and the space shuttle provided further opportunities of studying those effects (Sorrels et al., 2002). Using seismic records of the sonic boom by the space shuttle Columbia, returning to the California Edwards Air Force base, Kanamori et al. (1991) observed P-wave pulse across the Los Angeles basin, probably excited through the motion of high-rise buildings in response to the sonic boom. Sonic boom was also shown to induce ionospheric perturbations through the atmosphere-ionopshere coupling using data from GPS measurements (Calais and Minster, 1998).

4 Conclusion

It has been a traditional practice for seismologists to ignore the atmosphere, the outermost layer of the Earth. To a large extent, this has been justified because of its relatively small effect on seismograms.

On the other hand, because of the existence of the atmospheric layer, we receive some benefits. In addition to understanding the causes of noise, which shed some light on the mechanism in the atmosphere-ocean-solid earth interactions, one of the recent benefits has been the development of the correlation technique that allows us to retrieve Green's functions among pairs of stations. We can now obtain Green's functions for the solid Earth from the portions of seismograms that do not contain earthquake signals. This owes to the existence of noise and the development of theory on diffuse wavefield generated by noise.

Extending the analysis to include the atmospheric layer will increase opportunities to detect signals that are potentially useful for quantitative analysis of solid earth processes. Volcanic eruption is an obvious process as it directly generates atmospheric waves. Direct tsunami observation is also possible as surface displacement of ocean is not small and there are atmospheric waves that are coupled to this phenomenon. Shallow earthquakes also emit waves into the atmosphere which may become a useful source of information. We have probably scratched only the surface of a large body of useful phenomena in the atmosphere and as we develop the understanding of waves in the whole Earth system, we may discover many things that seismologists have missed in the past 100 years.

Nomenclature

Δg: Perturbation to gravitational acceleration

ΔP: Surface pressure perturbation

$\Delta\rho$: Density perturbation

f: Frequency in Hertz (Hz)

G: Gravitational constant (6.67×10^{-11} MKS unit)

g: Gravitational acceleration

ρ: Density

z: Vertical coordinate ($z = 0$ is surface and positive upward)

ζ: Ocean surface displacement

$\bar{\zeta}$: Averaged ocean surface displacement over its wavelength

$\mathbf{v}$: Velocity (three component vector)

C_s: Sound speed

γ: Specific heat ratio

k_x, k_y, k_z: Three components of wavenumber

ω: $2\pi f$

ω_g: Brunt-Väisälä frequency

ω_a: Acoustic cut-off frequency

N_e: Electron density in the upper atmosphere

e: electron charge

m_e: electron density

ϵ_0: Permittivity of vacuum

f_1: Primary carrier frequency of GPS

f_2: Secondary carrier frequency of GPS

Glossary

Acoustic Cut-off frequency: The frequency of radio waves below which acoustic waves are reflected back to Earth.

Barometer, Barograph: Instrument to measure atmospheric pressure.

Brunt-Väisälä frequency: When the medium is stably stratified, displaced particle in the medium starts to oscillate at this frequency. In an unstable medium, this frequency becomes complex.

GPS: Global Positioning System. Satellite-based positioning system. Two carrier frequencies, L1 (1.57542 GHz) and L2 (1.22760 GHz) are used.

Hum: Free oscillation peaks observed as background noise continuously. Frequency range is between 0.002 and 0.007 Hz approximately.

Infrasound: Low-frequency sound waves. Definition of frequency range is vague.

Ionosonde, Ionogram: Ionosonde is a land-based system to send radio waves upward and record reflection from the upper atmosphere. Ionogram is its record. Ionosonde has been used to monitor the state of upper atmosphere.

Microbarom: Atmospheric low-frequency waves which have close frequencies to microseisms. Believed to have the same origin with microseisms.

Microseism: Largest seismic noise in seismograms observed continuously. Frequency range is about 0.1-0.4 Hz (period 2-10 seconds). Ocean waves are known to generate this noise. The largest peak in seismic noise is found at about twice the frequency of ocean waves. Small amplitude noise at the frequency of ocean waves is called the primary-frequency microseisms, while 'microseisms' usually refer to the larger amplitude double-frequency microseisms. Doubling (and sometimes tripling) of frequency at the maximum amplitudes are believed to be caused by nonlinear mechanism in the Navier-Stokes equation.

NLNM: New Low Noise Model proposed by Peterson (1993).

Plasma frequency: Low frequency cut-off for radio wave propagation.

PREM: Preliminary reference Earth Model. One dimensional reference model published by Dzeiwonski and Anderson (1981).

Superconducting gravimeter: Sensitive gravimeter which uses superconductivity, typically Ni (niobium) ball floated in the magnetic field is used as its sensor.

TEC: Total electron density. An integral of electron density along a path.

References

[1] Afraimvich, E. L., N. P. Perevalova, A. V. Plotnikov, and A. M. Uralov, The shock-acoustic waves generated by earthquakes, *Ann. Geophys.*, 19, 395-409, 2001.

[2] Aki, K., Space and time spectra of stationary stochastic waves, with special reference to microtremors, *Bull. Earthq. Res. Inst.*, 35, 415-456, 1957.

[3] Aki, K., A note on the use of microseisms in determining the shallow structures of the earth's crust, *Geophysics,* 30, 665-666, 1965.

[4] Aki, K. and P. Richards, *Quantitative Seismology*, Freeman, New York, 1980.

[5] Arendt, S. and Fritts, D. C., Acoustic radiation by ocean surface waves, *J. Fluid Mech., 415*, 1-21, 2000.

[6] Artru, J., V. Ducic, H. Kanamori, P. Lognonne, and M. Murakami, Ionospheric detection of gravity waves induced by Tsunamis, *Geophys. J. Int.,* 160(3), 840-848, 2005.

[7] Artru, J., T. Farges, and P. Lognonne, Acoustic waves generated from seismic surface waves: propagation properties determined from doppler sounding observations and normal-mode modelling, *Geophys. J. Int.,* 158(3):1067-1077, 2004.

[8] Artru, J., P. Lognonne, and E. Blanc, Normal modes modelling of post-seismic ionospheric oscillations, *Geophys. Res. Lett.,* 28(4):697-700, 2001.

[9] Beauduin, R., P. Lognonne, J. P. Montagner, S. Cacho, J. F. Karczewski, and M. Morand, The effects of the atmospheric pressure changes on seismic signals or how to improve the quality of a station, *Bull. Seism. Soc. Am., 86*, No. 6, 1760-1769, 1996.

[10] Bedardm A. J., Atmospheric infrasound, *Physics Today*, 53, 32-37, 2000.

[11] Ben-Menahem, A., Source parameters of the Siberia explosion of June, 1908, from analysis and synthesis of seismic signals at four stations, *Phys. Earth Planet. Interi.*, 11, 1-35, 1975.

[12] Beroza, G. and T. Jordan, Searching for slow and silent earthquakes using free oscillations, *J. Geophys. Res., 95*, 2485-2510, 1990.

[13] Bilitza, D., International reference ionosphere 2000, *Radio Science*, 36(2):261-275, 2000.

[14] Blanc, E., Observations in the upper atmosphere of infrasonic waves from natural or artificial sources: A summary, *Ann. Geophys.*, 3(6):673-688, 1985.

[15] Bolt, B. Seismic air waves from the great Alaska earthquake, *Nature*, 202:1095-1096, 1964.

[16] Bolt, B. A. and T. Tanimoto, Atmospheric oscillations after the May 18, 1980 eruption of Mount St. Helens, *EOS*, Vol. 62, No. 23, 529, 1980.

[17] Boy, J. P., J. Hinderer, P.Gegout, Global atmospheric loading and gravity, *Phys. Earth Planet. Interi., 109*, 161-177, 1998.

[18] Bromirski, P. D., Vibrations from the "Perfect Storm", *Geochem. Geophys. Geosys., 2*, Paper number: 2000GC000119.

[19] Bromirski, P. D. and F. K. Duennebier, The near-coastal microseism spectrum: Spatial and temporal wave climate relationships, *J. Geophys. Res.*, 107, B8, 2166, 10.1029/2001JB000265, 2002.

[20] Bromirski, P. D., Flick, R. E., Graham, N., Ocean wave height determined from inland seismometer data: Implications for investigating wave climate change in the NE Pacific, *J. Geophys. Res., 104*, No. C9, 20,753-20,766, 1999.

[21] Calais, E., J. S. Haase, and J. B. Minster, Detection of ionospheric perturbations using a dense GPS array in Southern California, *Geophys. res. Lett.*, 30, 1628-1631, 2003.

[22] Calais, E. and B. Minster, GPS detection of ionospheric perturbations following the January 17, 1994, Northridge earthquake, *Geophys. Res. Lett.*, 22(9):1045-1048, 1995.

[23] Calais, E. and B. Minster, GPS, earthquakes, the ionosphere, and the Space Shuttle, *Phys. Earth Planet. Inter.*, 105(3-4):167-181, 1998.

[24] Campillo, M. and A. Paul, Long range correlations in the diffuse seismic coda, *Science, 299*, 547-549, 2003.

[25] Capon, J., Long-period signal processing results for LASA, NORSAR and ALPA, *Geophys. J. R. astr .Soc., 31*, 279-296, 1972.

[26] Cevaloni, G., The explosion of the bolide over lugo-di-romagna (Italy) on 19 january 1993, *Planetary and Space Science*, 42, 767-775, 1994.

[27] Cook, J. C., T. Gorforth, and R. K. Cook, Seismic and underwater responses to sonic boom, *J. Acoust. Soc. Am.*, 51(2):729-741, 1972.

[28] Cooper, R. I.B. and M. S. Longuet-Higgins, An experimental study of the pressure variations in standing water waves, *Proc. R. Soc. Lond.* A, 206, 424-435.

[29] Dahlen, A. F. and J. Tromp, *Theoretical Global Seismology*, Princeton University Press, Princeton, 1998.

[30] DasGupta, A., A. Das, D. Hui, K. K. Bandyopadhyay, and M. R. Sivaraman, Ionospheric perturbations observed by the GPS following the December 26th, 2004 Sumatra-Andaman earthquake, *Earth Planets Space, 58*(2), 167-172, 2006.

[31] Davies, J. B. and C. B. Archambeau, Modeling of atmospheric and ionospheric disturbances from shallow seismic sources, *Phys. Earth Planet. Inter.*, 105, 183-199, 1998.

[32] Davies, K. The measurement of ionospheric drifts by means of a Doppler shift technique, *J. Geophys. Res.*, 67, 4909-4913, 1962.

[33] Davies, K. and D. M. Baker, Ionospheric effects observed around the time of the Alaskan earthquake of March 28, 1964, *J. Geophys. Res.*, 70, 1251-1253, 1965.

[34] Derode, A., E. Larose, M. Tanter, J. de Rosney, A. Tourin, M. Campillo, and M. Fink, Recovering the Green's function from field-field correlations in an open scattering medium, *J. Acoust. Soc., 113*, 2973-2976, 2003.

[35] Donn, W., B. Naini, Sea wave origin of microbaroms and microseisms, *J. Geophys. Res., 78*, No. 21, 4482-4488, 1973.

[36] Donn, W., E. S. Posmentier, Ground-coupled air waves from the great Alaskan earthquake, *J. Geophys. Res.,*, 69, 5357, 1964.

[37] Drob, D. P., J. M. Picone, and M. Garces, Global morphology of infrasound propagation, *J. Geophys. Res.,* 108(D21), 4680, 2003.

[38] Duvall, T. L., S. M. Jefferies, J. W. Harvey, amd M. Pomerantz, *Nature, 362*, 430-432, 1993.

[39] Dziewonski, A. M. and D. L. Anderson, Preliminary Reference Earth Model, *Phys. Earth Planet. Int., 25*, 297-356, 1981.

[40] Ekström, G., Time domain analysis of Earth's long-period background seismic radiation, *J. Geophys. Res., 106*, No. B11, 26,483-26,493, 2001.

[41] Friedrich, A., F. Kruger, and K. Klinge, Ocean-generated microseismic noise located with the Grafenberg array, *J. of Seismology, 2*, 47-64, 1998.

[42] Graces, M.A., On the volcanic waveguide, *J. Geophys. Res.*, 102, B10, 22547-22564, 1997.

[43] Garces,M., C. Hetzer, M. Merrifield, M. Willis, and J. Aucan, Observations of surf infrasound in Hawaii, *Geophys. Res. lett.*, 30(24), 2264-2267, doi:10.1029/2003GL018614, 2003.

[44] Garces, M., P. Caron, C. Hetzer, A. Le Pichon, H. Bass, D. Drob, and J. Bhattacharyya, Deep infrasound from the Sumatra earthquake and tsunami, *Eos Trans. AGU, 86*(35), 317, 320, 2005.

[45] Grevemeyer, I., R. Herber, H.-H. Essen, Microseismological evidence for a changing wave climate in the northeast Atlantic Ocean, *Nature, 408*, 349-352, 2000.

[46] Gutenberg, B., Two types of microseisms, *J. Geophys. Res., 63*, 595-597, 1958.

[47] Haggerty, M. T., W. Y. Kim, and P. Martysevich, Infrasound detection of large mining blasts in Kazakstan, *Pure Appl. Geophys.*, 159, 1063-1079, 2002.

[48] Harkrider, D. and F. Press, The Krakatoa air-sea waves: an example of pulse propagation in coupled systems, *Geophys. J. R. Astr. Soc.*, 13, 149-159, 1967.

[49] Harkrider, D., Theoretical and observed acoustic-gravity waves from explosive sources in the atmosphere, *J. Geophys. Res.*, 69, 5295, 1964.

[50] Haubrich, R. A., W. Munk, and F. E. Snodgrass, Comparative spectra of microseisms and swell, *Bull. Seism. Soc. Am., 53,* 27-37, 1963.

[51] Heki K., Y. Otsuka, N. Choosakul, N. Hemmakorn, T. Komolmis, T. Maruyama, Detection of ruptures of Andaman fault segments in the 2004 great Sumatra earthquake with coseismic ionospheric disturbances, *J. Geophys. Res., 111*, B09313, doi:10.1029/2005JB004202, 2006.

[52] Hinderer, J. and D. Crossley, Time variations in gravity and inferences on the Earth's structure and dynamics, *Surveys in Geophys., 21*, 1-45, 2000.

[53] Hines, C. O., Internal atmospheric gravity waves at ionospheric heights, *Can. J. Phys.*, 38, 1441-1481, 1960.

[54] Hines, C. O., Gravity-waves in atmosphere, *Nature*, 239, 73-78, 1972.

[55] Igarashi, K., S. Kaminuma, I. Nishimuta, S. Okamoto, H. Kuroiwa, T. Tanaka, and T. Ogawa, Ionosphere and atmospheric disturbances around Japan caused by the eruption of Mount-Pinatubo on 15 June, 1991, *J. Atmosph. Terr. Phys.*, 56, 1227-1234, 1994.

[56] Il-Young, C., M.-S. Jun, J.-S. Jeon, and K. D. Min, Analysis of local seismo-acoustic events in the Korean peninsula, *Geophys. Res. Lett.*, 29, 10.1029/2001GL014060, 2002.

[57] Ishihara, Y., S. Tsukada, S. Sakai, Y. Hiramatsu, and M. Furumoto, The 1998 Miyako fireballs trajectory determined from shock wave records of a dense seismic array, *Earth Planets and Space*, 55, 9-12, 2003.

[58] Iyemori, T., M. Nose, D. Han,Y. Gao, M. Hashizume, N. Choosakul, H. Shinagawa, Y. Tanaka, M. Utsugi, A. Saito,H. McCreadie, Y. Odagi, and F. Yang, Geomagnetic

pulsations caused by the Sumatra earthquake on December 26, 2004, *Geophys. Res. Lett., 32*, L20807, doi:10.1029/2005GL024083, 2005.

[59] Johnson, J. B., Generation and propagation of infrasonic airwaves from volcanic explosions, *J. Volcano. Geotherm. Res.*, 121, 1-14, 2003.

[60] Kanamori, H., J. Mori, D. L. Anderson and T. H. Heaton, Seismic excitation by the space-shuttle columbia, *Nature*, 349, 781-782, 1991.

[61] Kanamori, H., J. Mori, and D. Harkrider, Excitation of atmospheric oscillations by volcanic eruptions, *J. Geophys. Res.*, 22, 21947-21961, 1994.

[62] Kobayashi, N. and K. Nishida, Continuous excitation of planetary free oscillations by atmospheric disturbances, *Nature, 395*, 357-360, 1998.

[63] Lacoss, R. T., E. J. Kelly, and M. N. Toksoz, Estimation of seismic noise structure using seismic arrays, *Geophysics, 34*, No. 1, 21-38, 1969.

[64] Lanyi, G. E., and E. Roth, A comparison of mapped and measured total ionospheric electron content using global positioning system and beacon satellite observation, *Radio Science*, 23, 483-492, 1988.

[65] Lay, T., H. Kanamori, C. J. Ammon, M. Nettles, S. N. Ward, R. C. Aster, S. L. Beck, S. L. Bilek, M. R. Brudzinski, R. Butler, H. R. DeShon, G. Ekstrm, K. Satake, and S. Sipkin, The great Sumatra-Andaman earthquake of 26 December 2004, *Science, 308*(5725), 1127 1133, doi: 10.1126/science.1112250, 2005.

[66] Lee, A. W., On the direction of approach of microseismic waves, *Proceedings of the Royal Society of London. Series A, Mathematical and Physical Sciences, 149*, No. 866, 183-199, 1935.

[67] LePichon, A., J. Guilbert, A. Vega, M. Garces, and N. Brachet, Ground-coupled air waves and diffracted infrasound from the Arequipa earthquake of June 23, 2001, *Geophys. Res. Lett,*, 29, 1886-1889, 2002.

[68] LePichon, A., J. Guilbert, M. Vallee, J.X. Dessa, and M. Ulziibat, Infrasonic imaging of the Kunlun mountains for the great 2001 China earthquake, *Geophys. Res. Lett,*, 30, 1814, 2003.

[69] Le Pichon, A., P. Herry, P. Mialle, J. Vergoz, N. Brachet, M. Garces, D. Drob, and L. Ceranna, Infrasound associated with 20042005 large Sumatra earthquakes and tsunami, *Geophys. Res. Lett., 32*, L19802, doi:10.1029/2005GL023893, 2005.

[70] Liu, J. Y., Y. B. Tsai, S. W. Chen, C. P. Lee, Y. C. Chen, H. Y. Yen, W. Y. Chang, and C. Liu, Giant ionospheric disturbances excited by the M9.3 Sumatra earthquake of 26 December 2004, *Geophys. Res. Lett., 33*, L02103, doi:10.1029/2005GL023963, 2006a.

[71] Liu, J.-Y., Y.-B. Tsai, K.-F. Ma, Y.-I. Chen, H.-F. Tsai, C.-H. Lin, M. Kamogawa, and C.-P. Lee, Ionospheric GPS total electron content (TEC) disturbances triggered by the 26 December 2004 Indian Ocean tsunami, *J. Geophys. Res., 111*, A05303, doi:10.1029/2005JA011200, 2006b.

[72] Lobkis, O. and R. Weaver, On the emergence of the Green's function in the correlations of a diffuse field, *J. Acoust. Soc. Am., 110*, 3011-3017, 2001.

[73] Lognonne, P., E. Clevede, and H. Kanamori, Computation of seismograms and atmospheric oscillations by normal-mode summation for a spherical earth model with realistic atmosphere, *Geophys. J. Int.*, 135, 388-406, 1998.

[74] Longuet-Higgins, M. S., A theory of the origin of microseisms, *Philos. Trans. R. Soc. Lond. A., 243*, 1-35, 1950.

[75] Mannucci, A. J., B. D. Wilson, D. N. Yuan, C. H. Ho, U. J. Lindqwister, and T. F. Runge, A global mapping technique for GPS-derived ionoispheric electron content measurements, *Radio Science,*, 33, 565-582, 1998.

[76] Mutschlecner, J. P. and R. W. Whitaker, Infrasound from earthquakes, *J. Geophys. res.*, 110 (D1), D01108, 2005.

[77] Najita, K., P. F. Weaver, and P. C. Yuen, A tsunami warning system using an ionospheric techniique, *Proceedings of the IEEE,* 62, 563-567, 1973.

[78] Najita, K. and P. C. Yuen, long-period oceanic Rayleigh wave group velocity dispersion curve from the doppler sounding of the ionosphere, *J. geophys. Res.*, 84, 1253-1260, 1979.

[79] Nawa, K., N. Suda, Y. Fukao, T. Sato, Y. Aoyama, K. Shibuya, Incessant excitation of the Earth's free oscillations, *Earth Planets Space, 50*, 3-8, 2000.

[80] Nawa, K., N. Suda, Y. Fukao, T. Sato, Y. Tamura, K. Shibuya, H. McQueen, H. Virtanen, J. Kaariainen, Incessant excitation of the Earth's free oscillations: global comparison of superconducting gravimeter records, *Phys. Earth Planet. Int., 120*, 289-297, 2000.

[81] Niebauer, T. M., Correcting gravity measurements for the effects of local air pressure, *J. Geophys. Res., 93*, No. B7, 7989-7991, 1998.

[82] Nishida, K., Y. Fukao, S. Watada, N. Kobayashi, M. Tahira, N. Suda and K. Nawa, T. Oi, T. Kitajima, Array observation of background atmospheric waves in the seismic band from 1 mHz to 0.5 Hz, *Submitted to Geophys J. Int*

[83] Nishida, K., N. Kobayashi, and Y. Fukao, Origin of Earth's ground noise from 2 to 20 mHz, *Geophys. Res. Lett., 29*, No. 10, 10.1029/2001/GL013862, 2002.

[84] Occhipinti, G., P. Lognonne, E. A. Kherani, and H. Hebert, Three-dimensional waveform modeling of ionospheric signature induced by the 2004 Sumatra tsunami, *Geophys. Res. Lett., 33*, L20104, doi:10.1029/2006GL026865, 2006.

[85] Okada, Hiroshi, *The Microtremor Survey Method*, Geophysical Monograph Series, Society of Exploration Geophysicists, No. 12, 2003.

[86] Okihiro, M., R. Guza, R. Seymour, Bound infragravity waves, *J. Geophys. Res., 97*, No. C7, 11,453-11,469, 1992.

[87] Y. Otsuka, N. Kotake, T. Tsugawa, K. Shiokawa,T.Ogawa, Effendy, S. Saito, M. Kawamura, T. Maruyama, N. Hemmakorn, and T. Komolmis, GPS detection of total electron content variations over Indonesia and Thailand following the 26 December 2004 earthquake, *Earth Planets Space, 58*(2), 159-165, 2006.

[88] Peltier, W. R. and C. O. Hines, Possible detection of tsunamis by a monitoring of ionosphere, *J. Geophys. Res.,* 81, 1995-2000, 1976.

[89] Peterson, J., Observation and modeling of background seismic noise, US Geol. Surv. Open-File Rept., Albuquerque, 1993.

[90] Phillips, O. M., *The dynamics of the upper ocean*, Camridge Unievrsity Press, Cambridge, 1977.

[91] Posmentier, E. S., A Thery of Microbaroms, *Geophys. J. R.Astr. Soc.*, 13, 487-501, 1967.

[92] Rabbel, W. and J. Zschau, Static deformations and gravity changes at the Earth's surface due to atmospheric loading, *J. Geophys., 56*, 81-99, 1985.

[93] Rhie, J., B. Romanowicz, Excitation of Earth's continuous free oscillations by atmosphere-ocean-seafloor coupling, *Nature, 431*, 552-556, 2004.

[94] Rickett, J. and J. Claerbout, Acoustic daylight imaging via spectral factorization: Helioseismology and reservoir monitoring, *The Leading Edge, 18*, 957-960, 1999.

[95] Roberts, D. H., J. A. Klobuchar, P. F. Fougere, and D. H. Hendrickson, A large-amplitude travelling ionospheric disturbance produced by the May 18, 1980, explosion of Mount St. Helens, *J. Geophys. Res.,* 87, 6291-6301, 1982.

[96] Row, R. V., Acoustic-gravity waves in the upper atmosphere due to a nuclear detonation and an earthquake, *J. Geophys. Res.,* 72, 1599-1610, 1967.

[97] Roult, G. and W. Crawford. Analysis of 'background' free oscillations and how to improve resolution by substracting the atmospheric pressure signal. *Phys. Earth Planet. Int., 121*, No. 3-4, 2000.

[98] Roux, P., K. G. Sabra, P. Gerstoft, W. A. Kupperman, and A. Roux, Ambient noise cross correlation in free space: Theoretical approach, *J Acoust. Soc., 117*, 79-84, doi:10.1121/1.1830673, 2005a.

[99] Roux, P., K. G. Sabra, P. Gerstoft, and W. A. Kupperman, P-waves from cross-correlation of seismic noise, *Geophys. Res. Lett, 32*, L19303, doi:10.1029/2005GL023803, 2005b.

[100] Sabra, K. G., P. Gerstoft, P. Roux, W. A. Kupperman, and M. Fehler, Surface wave tomography from microseisms in Soutehrn California, *Geophys. Res. Lett, 32*, L14311, doi:10.1029/2005GL023155, 2005.

[101] Sabra, K. G., P. Gerstoft, P. Roux, and W. A. Kupperman, Extracting time-domain Green's function estimates from ambient seismic noise, *Geophys. Res. Lett, 32*, L03310, doi:10.1029/2004GL021862, 2005.

[102] Saito, M., *Seismological Algorithms* edited by Doornbos, Academic Press, San Diego, 1988.

[103] Santo, T., Investigations into microseisms using the observational data of many stations in Japan (Part I) - on the origin of microseisms, *Bull. Earth. Research Inst.*, 37, 307-325, 1960.

[104] Sardon, E., A. Rius, N. Zarraoa, Estimation of the transmitter and receiver differential biases and the ionospheric total electron-content from Global POsitioning System observations, *Radio Science*, 29, 577-586, 1994.

[105] Shapiro, N. and M. Campillo, Emergence of broadband Rayleigh waves from correlations of the ambient seismic noise, *Geophys. Res. Lett, 31*, L07614, doi10.1029/2004GL019491, 2004.

[106] Shapiro, N., M. Campillo, L. Stehley and M. Ritzwoller, High-resolution surface-wave tomography from ambient seismic noise, *Science, 307*, 1615-1618, 2005.

[107] Snieder, R., Extracting the Green's function from the correlation of coda waves: A derivation based on stationary phase, *Phys. Rev. E, 69*, 046610, 2004.

[108] Song, Y. T., C. Ji, L.-L. Fu, V. Zlotnicki, C. K. Shum, Y. Yi, and V. Hjorleifsdottir, The 26 December 2004 tsunami source estimated from satellite radar altimetry and seismic waves, *Geophys. Res. Lett., 32*, L20601, doi:10.1029/2005GL023683, 2005.

[109] Sorrells, G. G., A preliminary investigation into the Relationship between Long-period noise and local fluctuations in the atmospheric pressure field, *Geophys. J. R. astr. Soc., 26*, 71-82, 1971.

[110] Sorrells, G., J. McDonald, Z. Der, and E. Herrin, Earth motion caused by local atmospheric pressure changes, *Geophys. J. R. astr. Soc., 26*, 83-98, 1971.

[111] Sorrells, G., J. Bonner, E. T. Herrin, Seismic precursors to space shuttle shock fronts, *Pure Appl. Geophys.*, 159, 1153, 1181, 2002.

[112] Suda, N., K. Nawa, Y. Fukao, Earth's background free oscillations, *Science, 279*, 2089-2091, 1998.

[113] Sutton, G. and N. Barstow, Ocean bottom microseisms from a distant supertyphoon, *Geophys. Res. Lett.*, 23, No. 5, 499-502, 1996.

[114] Takeuchi, H. and M. Saito, Seismic Surface Waves. In Bolt B. A. editor, *Methods in Computational Physics, 11* 217-295, Academic Press, New York, 1972.

[115] Tanimoto, T., Excitation of normal modes by atmospheric turbulence: source of long-period seismic noise. *Geophys. J. Int., 136*, 395-402, 1999.

[116] Tanimoto, T., Continuous free oscillations: Atmosphere-solid Earth coupling, *Annu. Rev. Earth Planet. Sci, 29*, 563-584, 2001.

[117] Tanimoto, T., The oceanic excitation hypothesis for the continuous oscillations of the Earth. *Geophys. J. Int., 160*, No. 1, 10.1111/j.1365-246X.2005.02491.x, 2005.

[118] Tanimoto, T., Excitation of normal modes by non-linear interaction of ocean waves, *Geophys. J. Int.*, in press, 2006.

[119] Tanimoto, T., J. Um, Cause of continuous oscillations of the Earth, *J. Geophys. Res., 104*, No. B12, 28,273-28,739, 1999.

[120] Tanimoto, T., J. Um, K. Nishida, N. Kobayashi, Earth's continuous oscillations observed on seismically quiet days, *Geophys. Res. Lett., 25*, No. 10, 1553-1556, 1998.

[121] Tanioka Y., Yudhicara, T. Kususose, S. Kathiroli, Y. Nishimura, S.-I. Iwasaki, and K. Satake, Rupture process of the 2004 great Sumatra-Andaman earthquake estimated from tsunami waveforms, *Earth Plants Space, 58*, 203-209, 2006.

[122] Van Dam, T. M., Wahr, J. M., Displacement of the Earth's surface due to atmospheric loading: Effects on gravity and baseline measurements. *J. Geophys. Res., 92*, No. B2, 1281-1286, 1987.

[123] van Tiggelen, B. A., Green function retrieval and time reversal in a disordered world, *Phys. Rev. Lett., 91*, 243904, 2003.

[124] Virieux, J., N. Garnier, E. Blanc, J. X. Dessa, Paraxial ray tracing for atmospheric wave propagation, *Geophys. Res. Lett.*, 31, 2004.

[125] Warburton, R. J., and Goodkind, J. M., The influence of barometric-pressure variations on gravity, *Geophys, J. R. astr. Soc., 48*, 281-292, 1977

[126] Watada, S., Near-source acoustic coupling between the atmosphere and the solid Earth during volcanic eruptions, PhD thesis, California Institute of Technology, Pasadena, 1995.

[127] Weaver, R. and O. Lobkis, Ultrasonics without a source. Thermal fluctuation correlations at MHz frequencies, *Phys. Rev. Lett., 87*, 134301, 2001.

[128] Webb, S., Broadband seismology and noise under the ocean, *Rev. Geophys, 36*, 105-142, 1998.

[129] Webb, S., X. Zhang, W. Crawford, Infragravity waves in the deep ocean, *J. Geophys. Res., 96*, No. C2, 2723-2736, 1991.

[130] Whipple, F. J. W., The great Siberian meteor and the waves, seismic and aerial, which it produced, *Royal Meteorological Society Quarterly Journal*, 56, 287-304, 1930.

[131] Widmer-Schnidrig, R., What can superconducting gravimeters contribute to normal-mode seismology? *Bull. Seismol. Soc. Am., 93*, No.3, 1370-1380, 2003.

[132] Wielandt, E. and J. M. Steim, A digital very-broad-band seismograph, *Ann. Geophys.* 4B, 227-232, 1986.

[133] Woodhouse, J. H., The calculation of the eigenfrequencies and eigenfunctions of the free oscillations of the earth and the sun, In: Doornbos, D. J. (Ed.), *Seismological Algorithms: Computational Methods and Computer Programs*, Acedemic Press, London,1988.

[134] Yeh, K. C., and C. H. Liu, *Theory of ionospheric waves*, New York, Academic Press, 1972.

[135] Young, J. M., and G. E. Greene, Anomalous infrasound generated by the Alaskan earthquake of 28 March 1964, *J. Acoust. Soc. Amer.*, 71, 334-339, 1982.

[136] Yuen, P. C., P. F. Weaver, R. K. Suzuki, and A. S. Furumoto, Continous travelling coupling between seismic waves and the ionosphere evident in May 1968 japan earthquake data, *J. Geophys. Res.,* 74, 2256-2264, 1969.

[137] Müller, T. and W. Zürn, Observation of gravity changes during the passage of cold fronts, *J. Geophys., 53,* 155-162, 1983.

[138] Zürn, W., R. Widmer, On noise reduction in vertical seismic records below 2 mHz using local barometric pressure, *Geophys. Res. Lett., 22*, No. 24, 3537-5340, 1995.

Figure Caption

Figure 1: New Low Noise Model by Peterson (1993). Power Spectral Density (PSD) in unit for acceleration is used for this plot. Frequency range is from 1/10000 (Hz) to 10 Hz.
Figure 2: (top) Original gravity signal from Warburton and Goodkind (1977). Data were recorded by super-conducting gravimeter. (Middle) gravity signal after tidal signal removal. (Bottom) Barometer signal, which correlates well with the trace in the middle.

Figure 3: Barometric data (pressure) from five stations in North and South America. Analysis was performed for 20-day long signals and spectral amplitudes were averaged over 0.2 mHz range. Solid circles denote 1/f trend.
Figure 4: Averaged acceleration PSD from 11 stations, distributed from various parts of the world, is shown at top. Circles in the top panel are NLNM. Spectra in the small box (top) are enlarged in the bottom panel. Each modal peak is shown to match the eigenfrequency of fundamental spheroidal mode (vertical lines in the bottom panel).

Figure 5: Significant Wave Height data from TOPEX-POSEIDON data. Data from two selected periods, one in January (top) and the other in July (bottom), are shown. In January, ocean waves are energetic in the mid-latitude region in the northern hemisphere, while ocean waves in the southern hemeisphere become energetic in July.

Figure 6: Domains of existence of waves in the solid Earth, ocean and atmosphere. This figure represents the set of free oscillation modes obtained using standard minos software (Woodhouse 1988) for a Earth model composed of PREM for solid Earth and U.S. Standard Atmosphere 1976 up to 86 km of altitude. Green dots: seismic spheroidal modes; Red dots: "tsunami" mode (corresponding to the 3-km ocean layer in PREM); Blue dots: acoustic and gravity mode. As minos software has a free boundary at the top of the model, some obvious errors exists: the atmospheric mode spectrum is not in general discrete because there is no upper-boundary condition, and furthermore, the lowest acoustic branch shown on this plot would correspond to the non physical surface atmospheric mode at the top of the model.

Figure 7: Typical mid-latitude electron density profile in the ionosphere. Profiles were obtained using the International Reference Ionosphere model (Bilitza, 2000). Main ions species are indicated, (dashed lines are their contribution to ionization), and the plasma frequencies (Eq. 11) corresponding to different electron densities are indicated.

Figure 8: Infrasound record from the I34MN IMS infrasound array (Mongolia) after the 2001 Kunlun earthquake (Northern China, Ms 8.1 on November 14, 2001). Bottom panel: Atmospheric pressure fluctuations recorded filtered between 0.05 and 4 Hz.Top 2 panels: the color scales indicate the values of the azimuth and the trace velocity measured at the infrasound station. Y-axis correspond to frequencies from 0.05 to 1 Hz . In the first part of the signal, coherent wave trains referred as Group A are related to local seismically coupled air waves. Due to the coupling at the earth-air interface, the horizontal trace velocity of the ground-coupled air waves and the seismic waves are identical (greater than 3 km/s). Group B corresponds to the propagation of infrasonic waves backscattered by the Kunlun mountain range.

Figure 9: Schematic view of atmospheric waves generated after an earthquake

Figure 10: Seismogram and Doppler sounding record (2 altitudes: 168 and 186 km) taken in France after Chi-Chi earthquake. Both traces are band-pass filtered between 1 and 50 mHz.

Figure 11: Observed signal for the June 23rd, 2001 tsunami (initiated offshore Peru): TEC variations plotted at the ionospheric piercing points. A wave-like disturbance is propagating towards the coast of Honshu. This perturbation presents the expected characteristics of a tsunami induced gravity waves, and arrives approximately at the same time as the tsunami wave itself.

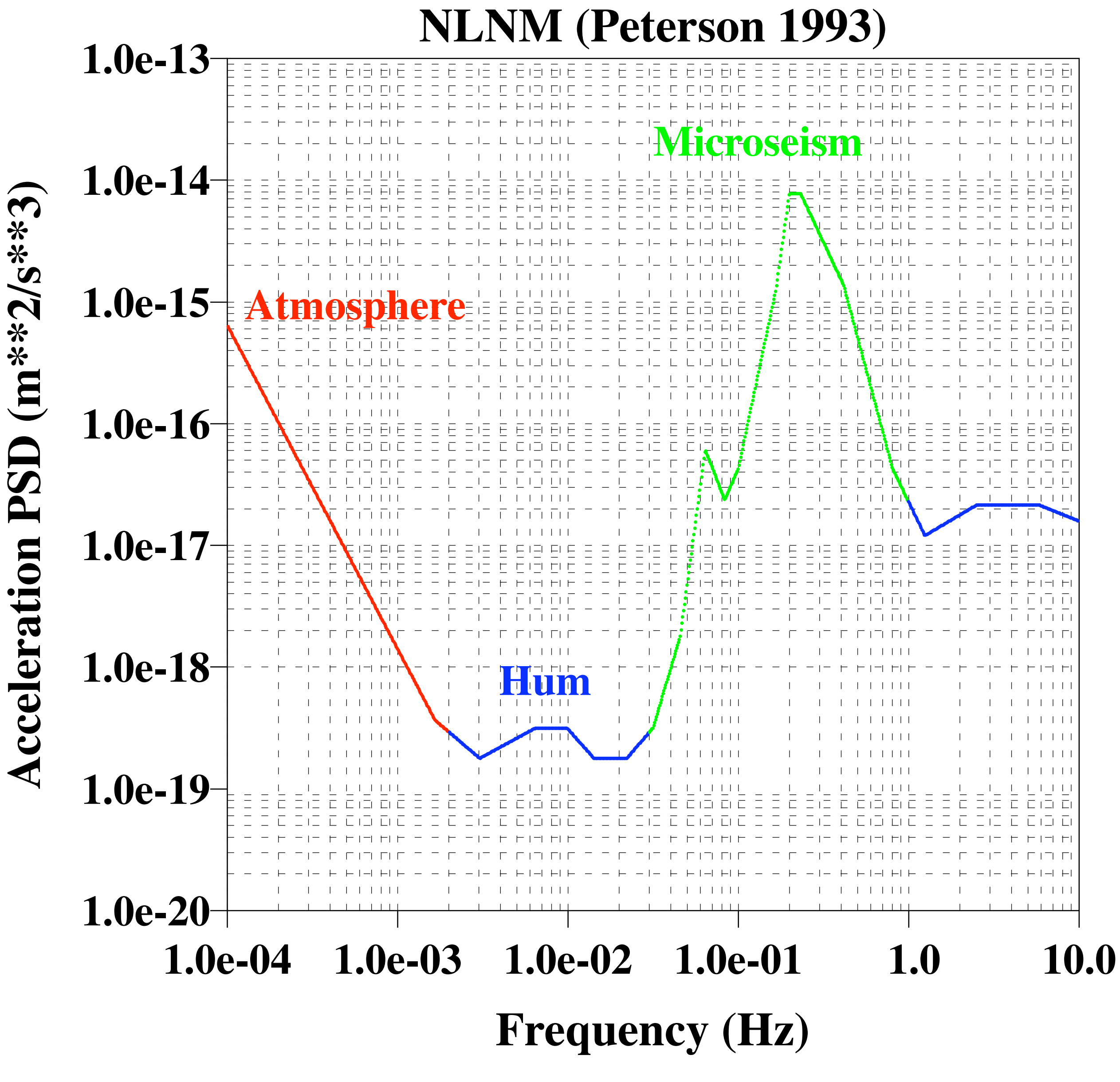

NLNM (Peterson 1993)
Acceleration PSD (m**2/s**3)
1.0e-13
1.0e-14
1.0e-15
1.0e-16
1.0e-17
1.0e-18
1.0e-19
1.0e-20
Microseism
Atmosphere
Hum
1.0e-04
1.0e-03
1.0e-02
1.0e-01
1.0
10.0
Frequency (Hz)

Figure 1

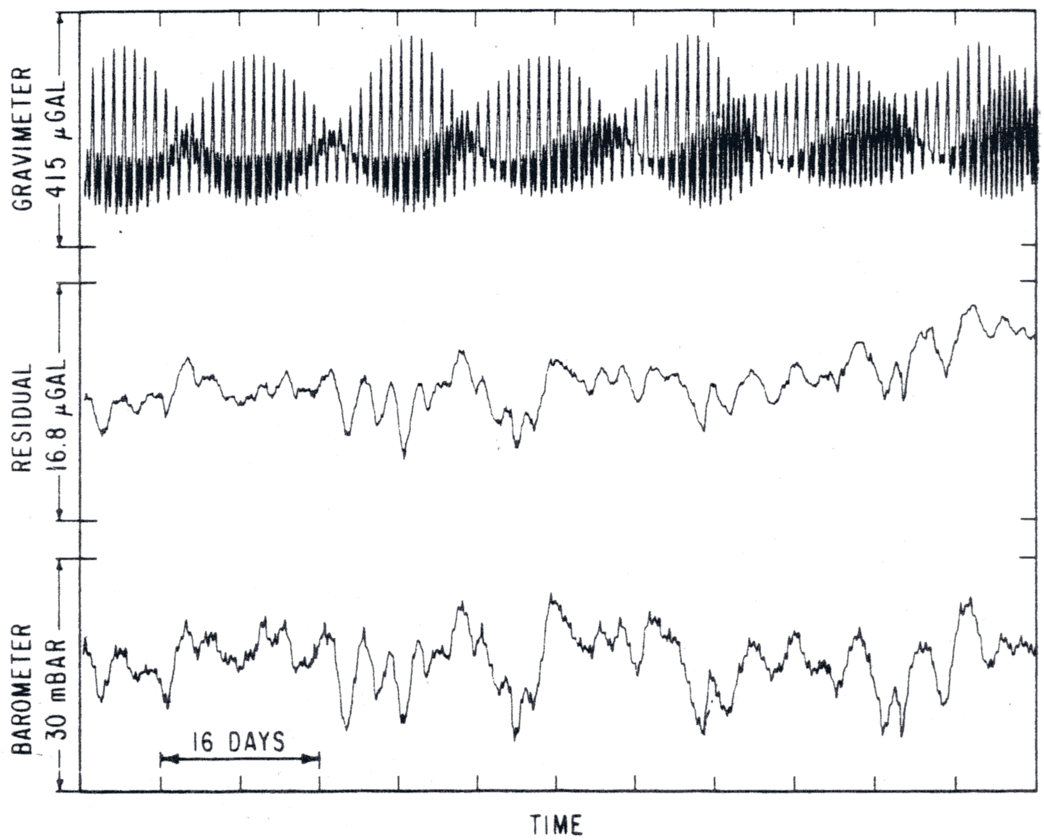
GRAVIMETER
415 μGAL
RESIDUAL
16.8 μGAL
BAROMETER
30 mBAR
16 DAYS
TIME

Figure 2

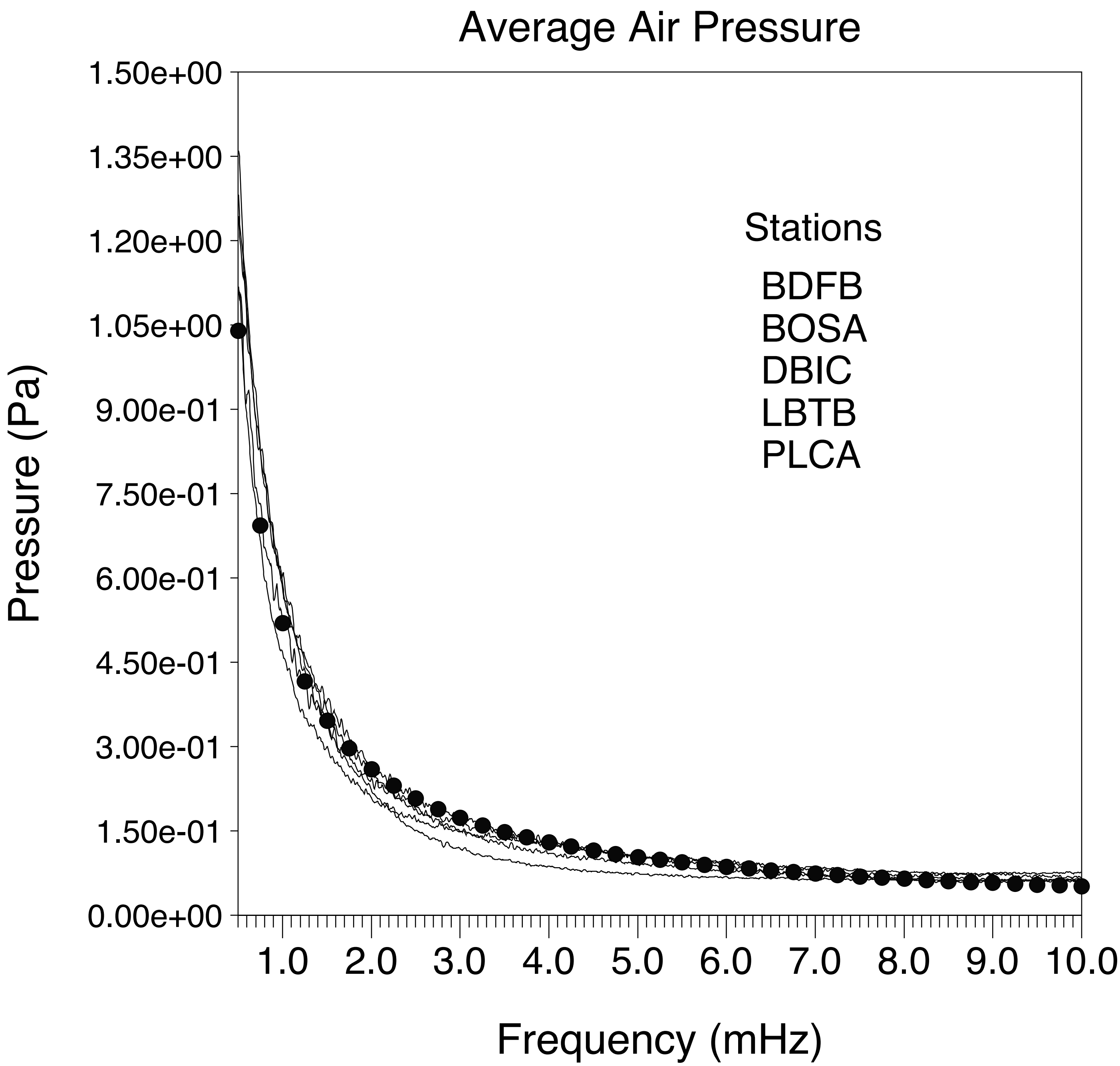
Average Air Pressure
1.50e+00
1.35e+00
1.20e+00
1.05e+00
9.00e-01
7.50e-01
6.00e-01
4.50e-01
3.00e-01
1.50e-01
0.00e+00
Pressure (Pa)
Stations
BDFB
BOSA
DBIC
LBTB
PLCA
1.0
2.0
3.0
4.0
5.0
6.0
7.0
8.0
9.0
10.0
Frequency (mHz)

Figure 3

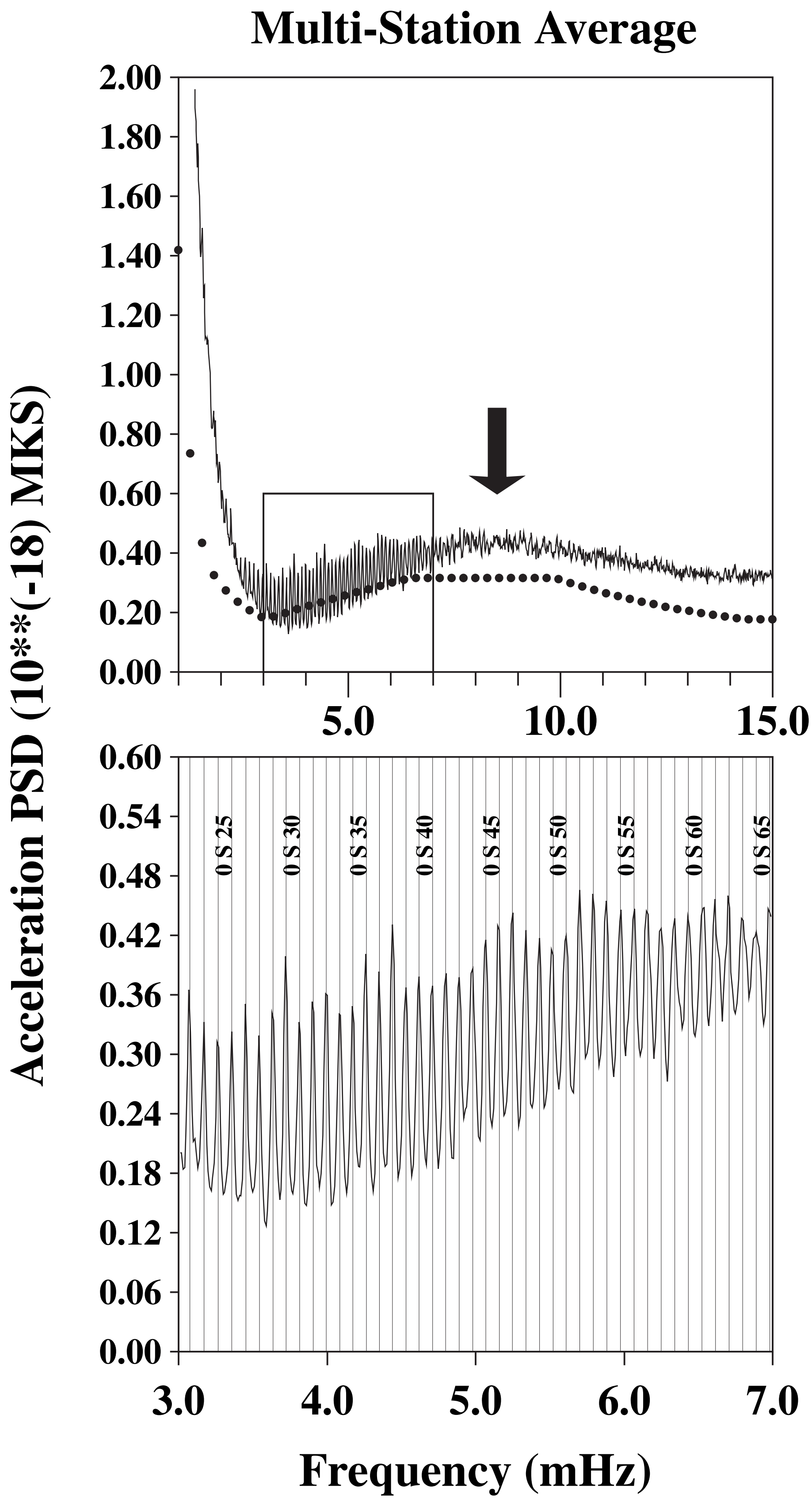
Multi-Station Average
Acceleration PSD (10**(-18) MKS)
2.00
1.80
1.60
1.40
1.20
1.00
0.80
0.60
0.40
0.20
0.00
5.0
10.0
15.0
0.60
0.54
0.48
0.42
0.36
0.30
0.24
0.18
0.12
0.06
0.00
0 S 25
0 S 30
0 S 35
0 S 40
0 S 45
0 S 50
0 S 55
0 S 60
0 S 65
3.0
4.0
5.0
6.0
7.0
Frequency (mHz)

Figure 4

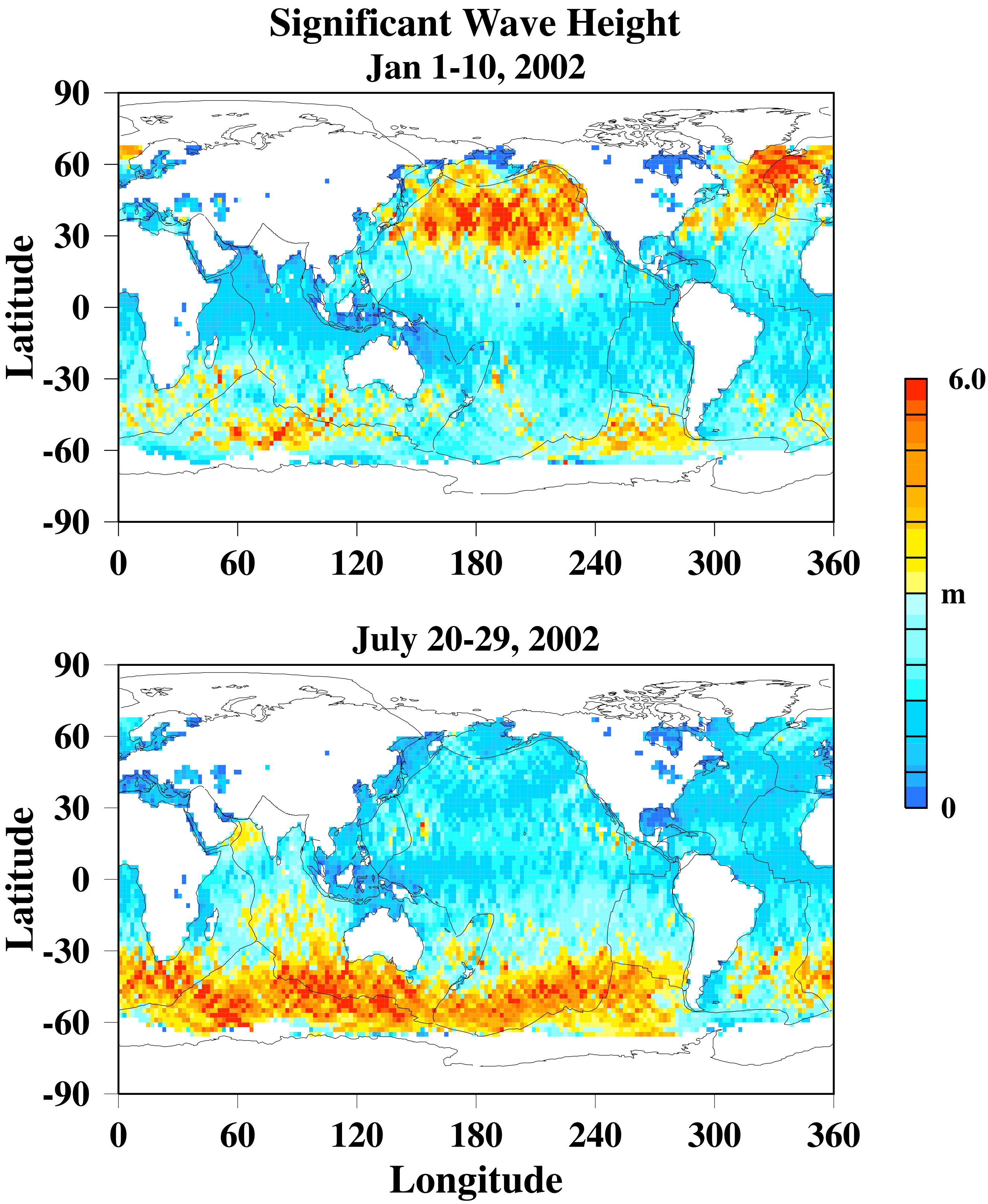

Significant Wave Height
Jan 1-10, 2002
July 20-29, 2002
Latitude
Longitude
90
60
30
0
-30
-60
-90
0
60
120
180
240
300
360
6.0
m
0

Figure 5

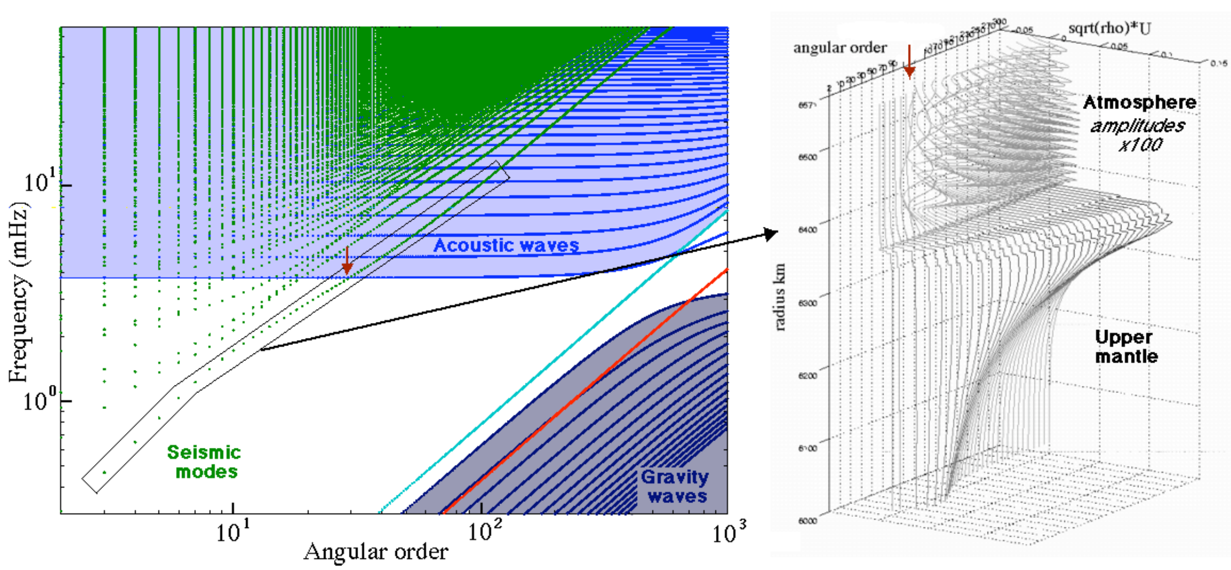
Frequency (mHz)
Angular order
Acoustic waves
Seismic modes
Gravity waves
angular order
sqrt(rho)*U
radius km
Atmosphere
amplitudes x100
Upper mantle

Figure 6

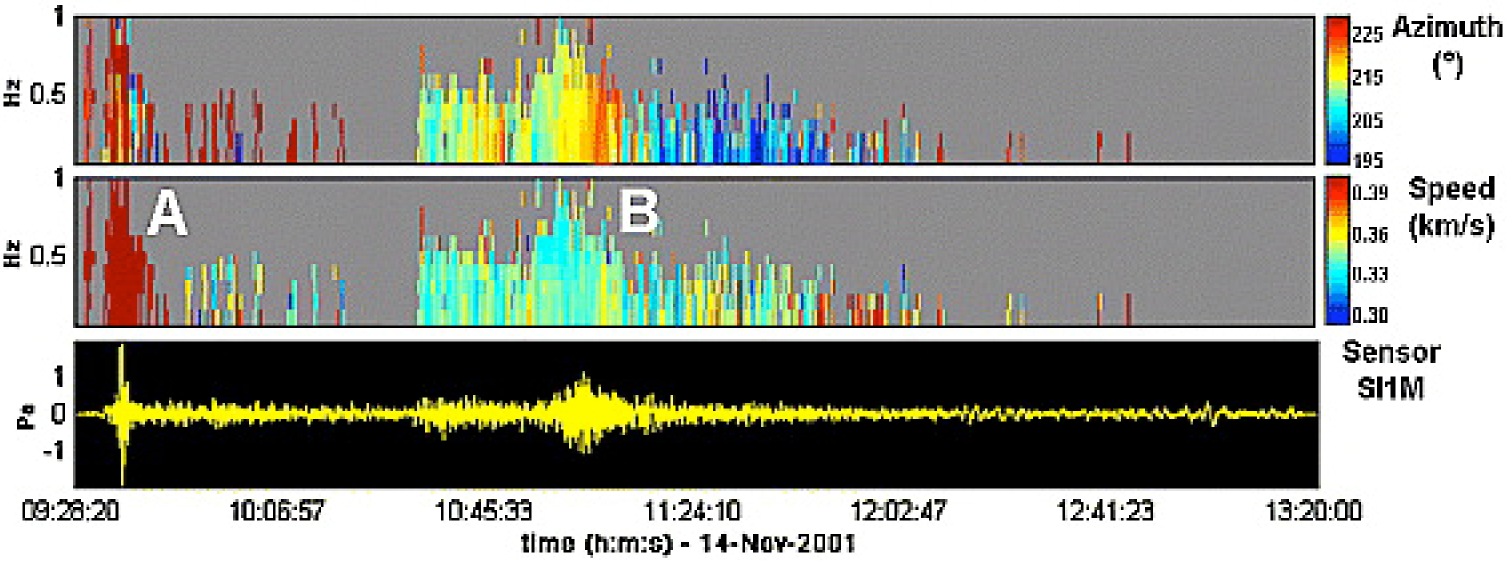
Azimuth (°)
225
215
205
195
Speed (km/s)
0.39
0.36
0.33
0.30
A
B
Hz
0.5
1
Pa
0
-1
Sensor SI1M
09:28:20
10:06:57
10:45:33
11:24:10
12:02:47
12:41:23
13:20:00
time (h:m:s) - 14-Nov-2001

Figure 7

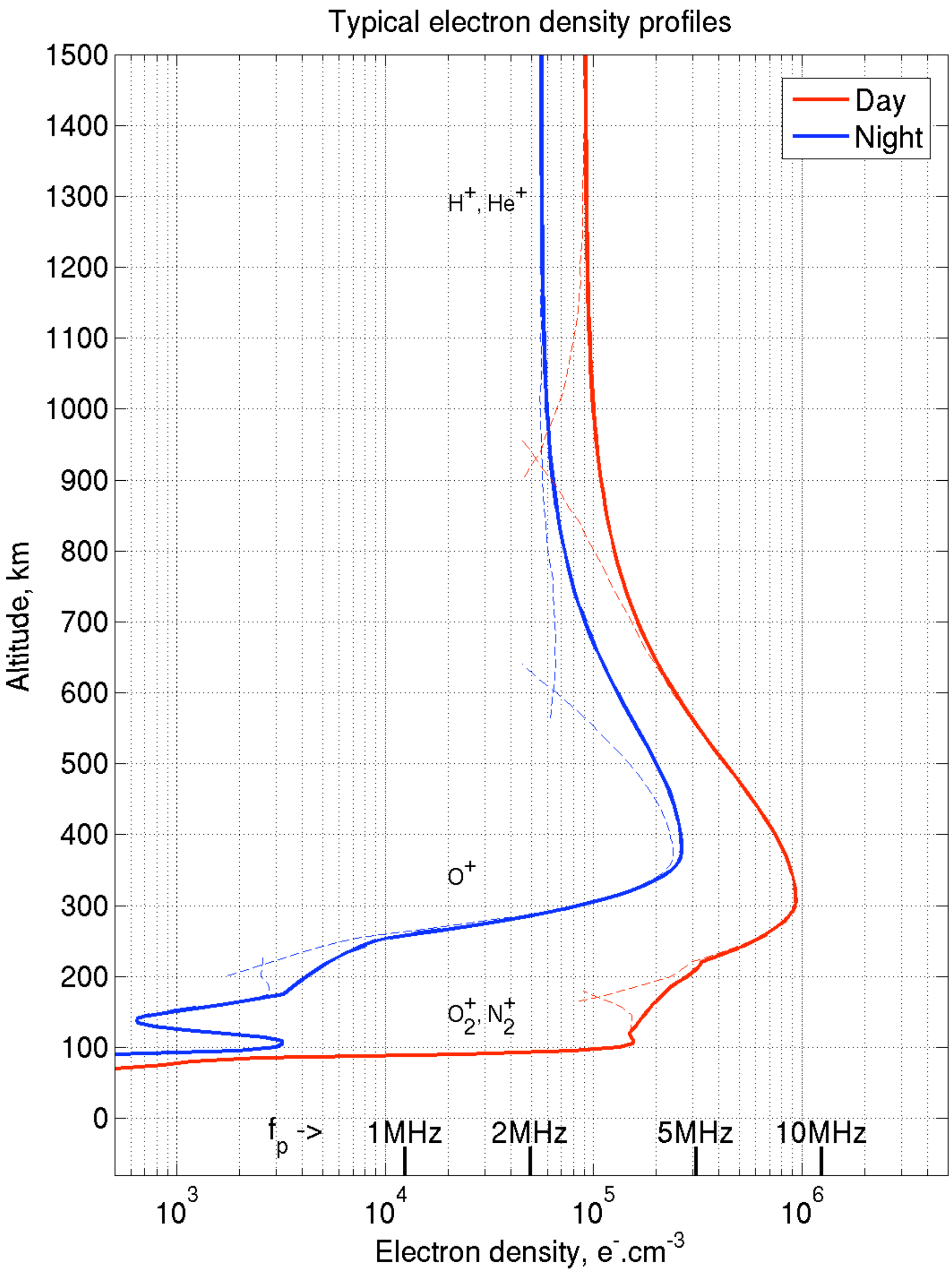
Typical electron density profiles
Day
Night
H+, He+
O+
O2+, N2+
fp ->
1MHz
2MHz
5MHz
10MHz
Altitude, km
Electron density, e-.cm-3

Figure 8

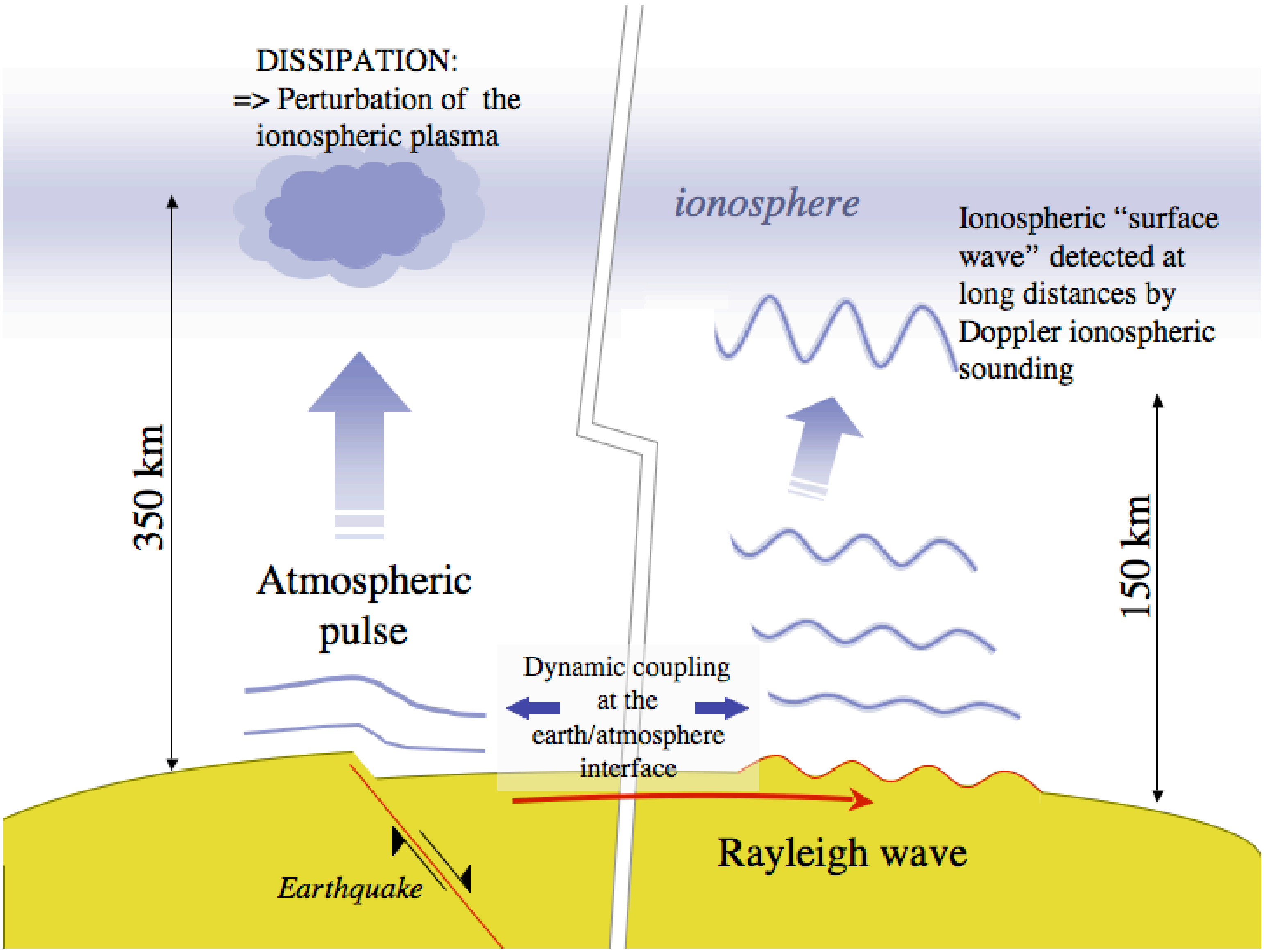
DISSIPATION:
=> Perturbation of the ionospheric plasma
ionosphere
Ionospheric "surface wave" detected at long distances by Doppler ionospheric sounding
350 km
150 km
Atmospheric pulse
Dynamic coupling at the earth/atmosphere interface
Rayleigh wave
Earthquake

Figure 9

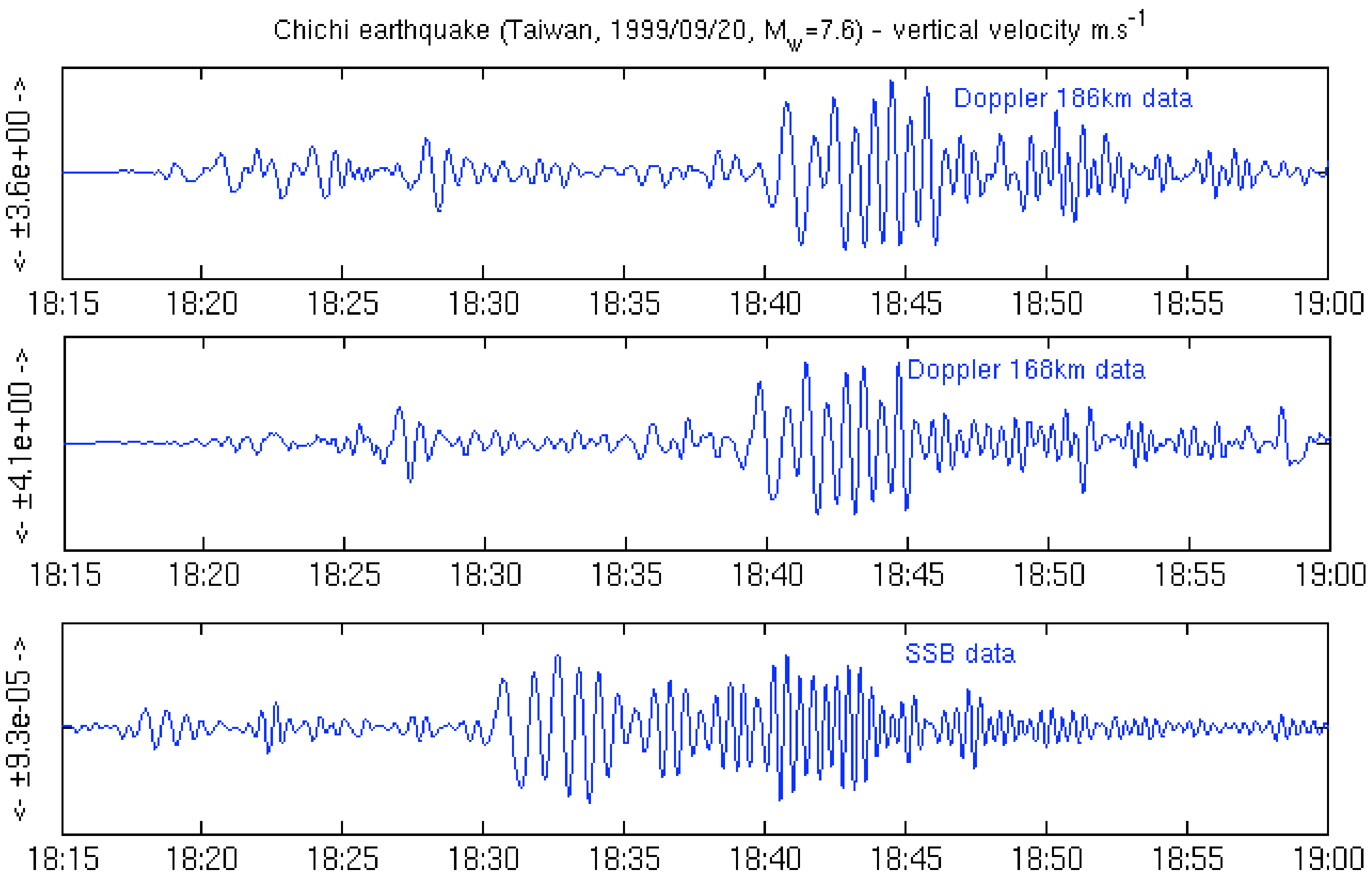
Chichi earthquake (Taiwan, 1999/09/20, M_W=7.6) - vertical velocity m.s^{-1}
<- ±3.6e+00 ->
Doppler 186km data
<- ±4.1e+00 ->
Doppler 166km data
<- ±9.3e-05 ->
SSB data
18:15
18:20
18:25
18:30
18:35
18:40
18:45
18:50
18:55
19:00

Figure 10

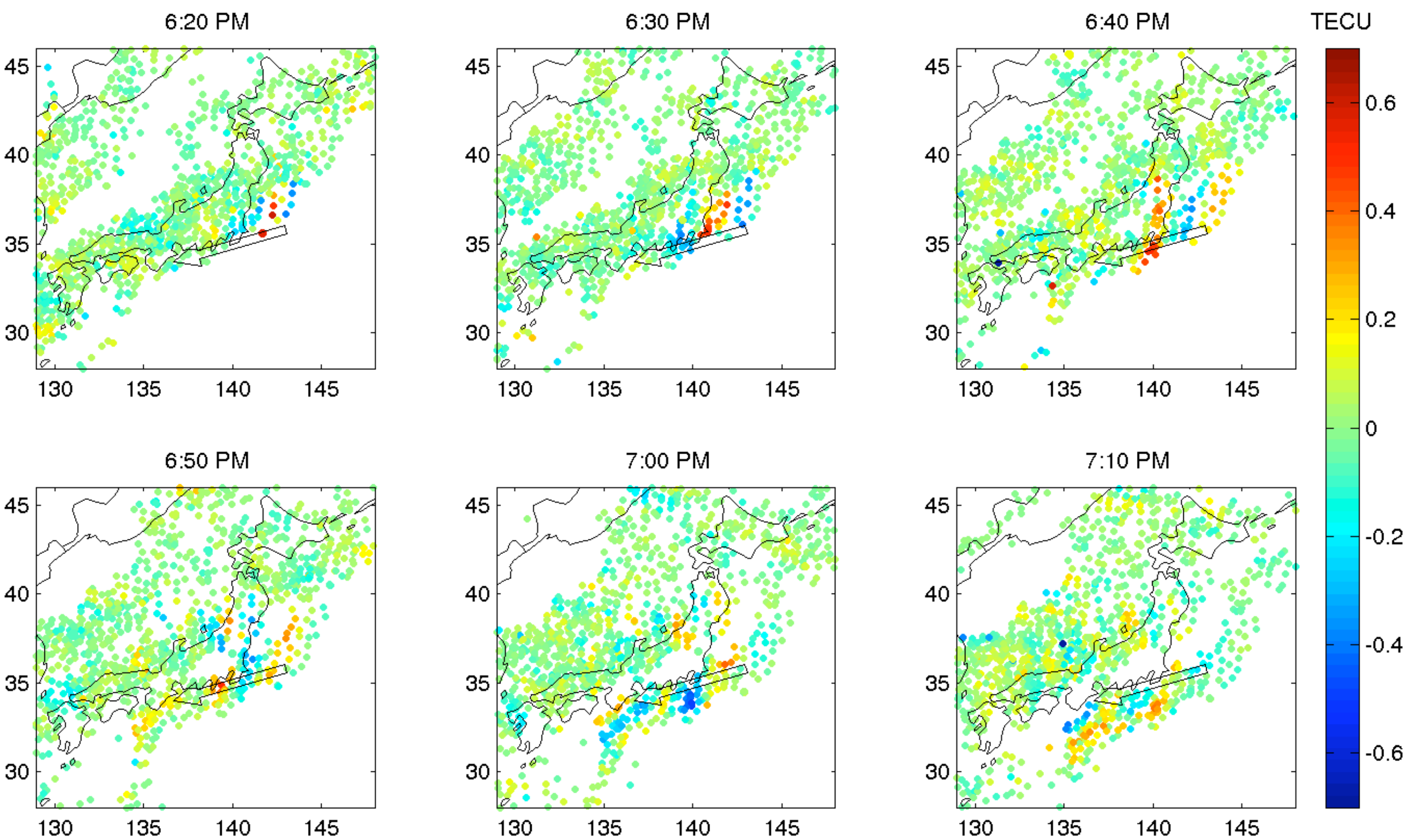
6:20 PM
6:30 PM
6:40 PM
6:50 PM
7:00 PM
7:10 PM
TECU
45
40
35
30
130
135
140
145
0.6
0.4
0.2
0
-0.2
-0.4
-0.6

Figure 11